Julià Sapé, Ma. Margarita; Candiota Silveira, Ana Paula; Arús i Caraltó, Carles. «Cancer metabolism in a snapshot : MRS(I)». NMR in Biomedicine, Vol. 32, Issue 10 (October 2019), art. e4054. DOI 10.1002/nbm.4054

Cancer metabolism in a snapshot: MRS(I)

Margarida Julià-Sapé1,2,3#, Ana Paula Candiota1,2,3#, Carles Arús2,1,3 *

1 Centro de Investigación Biomédica en Red en Bioingeniería, Biomateriales y Nanomedicina (CIBER-BBN), Cerdanyola del Vallès, Spain

2 Departament de Bioquímica i Biologia Molecular, Unitat de Bioquímica de Biociències, Universitat Autònoma de Barcelona (UAB), Cerdanyola del Vallès, Spain

3 Institut de Biotecnologia i de Biomedicina (IBB), Universitat Autònoma de Barcelona (UAB), Cerdanyola del Vallès, Spain

#Contributed equally

*Corresponding author

Funding information: Centro de Investigación Biomédica en Red, Grant/Award Number: CB06-01-0010; Ministerio de Economía y Competitividad (MINECO), Grant/Award Number: MOLIMAGLIO (SAF2014-52332-R

Abstract

The contribution of MRS(I) to the in vivo evaluation of cancer-metabolism-derived metrics, mostly since 2016, is reviewed here. Increased carbon consumption by tumour cells, which are highly glycolytic, is now being sampled by 13C magnetic resonance spec- troscopic imaging (MRSI) following the injection of hyperpolarized [1-13C] pyruvate (Pyr). Hot-spots of, mostly, increased lactate dehydrogenase activity or flow between Pyr and lactate (Lac) have been seen with cancer progression in prostate (preclinical and in humans), brain and pancreas (both preclinical) tumours. Therapy response is usu- ally signalled by decreased Lac/Pyr 13C-labelled ratio with respect to untreated or non- responding tumour. For therapeutic agents inducing tumour hypoxia, the 13C-labelled Lac/bicarbonate ratio may be a better metric than the Lac/Pyr ratio. 31P MRSI may sample intracellular pH changes from brain tumours (acidification upon antiangiogenic treatment, basification at fast proliferation and relapse). The steady state tumour metabolome pattern is still in use for cancer evaluation. Metrics used for this range from quantification of single oncometabolites (such as 2-hydroxyglutarate in mutant IDH1 glial brain tumours) to selected metabolite ratios (such as total choline to N-acetylaspartate (plain ratio or CNI index)) or the whole 1H MRSI(I) pattern through pattern recognition analysis. These approaches have been applied to address different questions such as tumour subtype definition, following/predicting the response to therapy or defining better resection or radiosurgery limits.

Keywords

animal model study, cancer, cellular and molecular cancer imaging, hyperpolarized C-13, MRS and MRSI methods, phosphorus MRS/MRSI

Abbreviations used: 2HG, 2-hydroxyglutarate; ADC, apparent diffusion coefficient; CEST, chemical exchange saturation transfer; Cho, choline; Cit, citrate; CNI, choline-to-NAA index; Cr, creatine; ERG, erythroblast transformation-specific (ETS) transcriptional factor-related gene; GB, glioblastoma; GEM, genetically engineered mouse; Glx, glutamate and glutamine; GPC, glycerophosphocholine; HIF, hypoxia-inducible factor; HR-MAS, high resolution magic angle spinning; IDH, isocitrate dehydrogenase; Lac, lactate; LDH, lactate dehydrogenase; LDHA, lactate dehydrogenase isoform A; ML, mobile lipid; MRSI, magnetic resonance spectroscopic imaging; mTOR, mammalian target of rapamycin; NAA, N-acetylaspartate; NADP+/NADPH, nicotinamide adenine dinucleotide 2'-phosphate, oxidized/reduced form; PA, polyamine; PCho, phosphocholine; pHe, extracellular pH; pHi, intracellular pH; PKM2, pyruvate kinase isoform M2; Pyr, pyruvate; ROI, region of interest; SDH, succinate dehydrogenase; SNR, signal-to-noise ratio; Spm, spermine; SUCCES, Succinate Estimation by Spectroscopy; SV, single voxel; T2W, T2 weighted; TCA, tricarboxylic acid; tCho, total choline; tCr, total creatine; TMZ, temozolomide; VOI, volume of interest; wt, wild type

Temporal and thematic boundaries of the topics covered

The authors of this review declare at the outset that there is no intention of being exhaustive or systematic. The temporal boundaries reviewed will be modest: only relevant literature since 2016, chosen according to our bias. Earlier work or reviews will only be referred to in order to put recent findings in due perspective. Authors hope that this summary will give readers a picture of how far cancer metabolism analysis with MRS(I) has advanced and, perhaps, why it is not advancing further.

For quite a long time MRS, rather than MRI, has been the only approach able to evaluate cancer metabolism. Nevertheless, the MRI-derived information related to cancer metabolism should not be forgotten: consider for example the chemical exchange saturation transfer (CEST) effect caused by exchangeable protons in water-derived images of glucose uptake and metabolism in tumours.1,2 However, apart from these CEST- related studies, we should acknowledge that most information about cancer metabolism using MR still refers to MRS(I) acquisitions, which are the ones dealt with in our text.

Supplementary Figure 1 shows a PUBMED search illustrating the different proportions of articles investigating several cancer types through MRS(I) approaches. The retrieved information can help understand the questions that users expect to be answered by MR. It seems clear that users of the MR methodology perceive, or expect, that in vivo MRS(I) will deliver useful information about spatial heterogeneity in prostate and brain cancer, but not in breast cancer. On the other hand, single voxel (SV) MRS still seems to play a role in brain and breast cancer, but not so much for prostate cancer. Ex vivo HRMAS studies in the period investigated in this review seem to be mostly used in breast and prostate cancer, and there is a recent review on the matter that analyses its use in detail.3

Cancer produces a series of anatomical and metabolic changes: emerging hallmarks

Cancer development and progression depends on the metabolic reprogramming caused by oncogenic mutations.4 Cancer cells are known to be highly proliferative, and the metabolism adaptation of cancer cells has the ultimate goals of survival and sustaining proliferation. This includes the ability to gather nutrients from a sometimes limited environment for viability maintenance and new biomass building. Pavlova and Thompson5 have organized known cancer-associated metabolic changes into six hallmarks: (a) deregulated uptake of glucose and amino acids, (b) use of opportunistic modes of nutrient acquisition, (c) use of glycolysis/TCA (tricarboxylic acid) cycle intermediates for biosynthesis and NADPH (nico- tinamide adenine dinucleotide 2'-phosphate, reduced form) production, (d) increased demand for nitrogen, (e) alterations in metabolite-driven gene regulation and (f) metabolic interactions with the microenvironment. The specific hallmarks exhibited by an individual tumour may contribute to better classification and help in treatment monitoring due to the relationship between malignant transformation, response to treatment and changes observable in tissue metabolism. Needless to say, the neoplastic process is also accompanied by changes at the level of microenviron- ment, cellular microstructure and peripheral vascular networks. The ability to sample all or most of these transformations is of crucial importance in a cancer patient's management, not only for early diagnosis but also for the non-invasive evaluation of the tumour response to a given therapy. It is worth stressing that many therapies can target cancer metabolism, and the changes triggered in endogenous metabolites should be detectable before changes in tumour volume are observed. Last but not least, it is important to bear in mind that MR techniques are essentially sampling a volume of tissue that is not entirely composed by tumour cells.6-8 Indeed in brain tumours such as glioblastoma (GB), the percentage of tumour- associated macrophages can be as high as 30% of the abnormal mass,9 constituting a cell population with its own metabolic features and differentially affected by therapy.

Advantages of sampling the metabolome by MRI/MRS(I)

Magnetic resonance is a non-invasive, non-ionizing, non-destructive technique, offering a high level of anatomic detail (MRI) and information about metabolomics/chemical environment (MRS(I)), being in general the method of choice for in vivo tumour diagnosis and follow-up. As an advantage over methods involving ionizing radiation, repeated MR measurements can be made in longitudinal experiments without cumulative harm to subjects. However, in vivo MR studies are only sensible if in vitro evaluations are not feasible or relevant, because the resolution and sensitivity level obtained are not comparable. In fact, most of the time ex vivo studies (i.e. high resolution magic angle spinning (HR-MAS) of biopsies) are performed to confirm or explain changes seen in in vivo studies.3,10-19 However, interest in MRS(I) is increasing for clinical applica- tions and research due to its ability to provide information about tissue spatial heterogeneity through collection of spectroscopic data and spatial distribution of metabolites, as well as their changes. In this respect, MRS(I) protocols can provide relevant information on surrogate biomarkers of disease diagnosis and prognosis, helping surgery and radiation planning, as well as predicting survival and treatment response.

Next, we will consider some specific aspects in which cancer metabolism studied by MR is contributing to increase our understanding of its progression and helping to control and eventually cure it.

MRS(I)- detectable metabolic hallmarks of cancer: applications to grading and/or therapy response

Carbon consumption

Cancers are highly glycolytic; they can be highly glutaminolytic too, and this usually requires high lactate dehydrogenase (LDH) content and activity.20-22 Accordingly, one would expect a tumour to demonstrate increased LDH-catalysed substrate flow through the enzyme, from pyruvate (Pyr) to lactate (Lac), with concomitant NAD+ (nicotinamide adenine dinucleotide, oxidized form) regeneration, when compared with normal tissue or when progressing to higher grade. This metric is a usually accepted surrogate biomarker of increased LDH activity and has been described in Reference 23 in a preclinical model of genetically engineered mice (GEMs) that spontaneously develop pancreatic cancer, undergoing several intermediary stages (Figure 1). Hyperpolarized 13C MRS(I) has been also used to monitor the increase in the Lac/Pyr ratio with progression to tumour,24 which can be transformed onto magnetic resonance spectroscopic imaging (MRSI)-derived images, for example in pancreatic cancer (Supplementary Figure 2).

Conceptually similar observations have been described for the TRAMP preclinical model of prostate cancer25 with significantly increased Pyr to Lac flux (a parameter known as kPL) in high-grade compared with low-grade tumours monitored by hyperpolarized 13C MRSI after the injection of hyperpolarized [1-13C]Pyr. This correlated with a more than twofold proliferation increase (percentage of Ki67+ cells) and close to twofold lactate dehydrogenase isoform A (LDHA) expression increase in high-grade versus low-grade tumours, ex vivo.

In a first-in-human study performed with 31 prostate cancer patients receiving an escalation dose design with injected hyperpolarized [1-13C] Pyr,26 a high Lac/Pyr ratio identified cancer in one of the bilaterally hyperpolarized 13C MRSI-detected regions that were inconspicuous by classical MR approaches (T2-weighted (T2W) or diffusion-weighted imaging) or 1H-based MRSI (Supplementary Figure 3).

Accordingly, a tumour responding to a particular therapy should show decreased LDH activity when injecting hyperpolarized Pyr. This effect has been shown27 in a case report of a patient with prostate-specific antigen of 25.2 ng/mL and Gleason 4 + 5 prostate adenocarcinoma on biopsy, who showed response to androgen deprivation therapy after 6 weeks of treatment, when only modest changes of abnormal prostate volume tissue and apparent diffusion coefficient (ADC) could be seen (Figure 2).

These results are in agreement with previous findings on preclinical GB models,28 for which the Lac/Pyr ratio after injection of hyperpolarized Pyr was seen to significantly decrease after combined dual PI3K/mTOR (mammalian target of rapamycin) inhibitor and temozo- lomide (TMZ) treatment, and before changes in tumour size or total choline (tCho) in the 1H MRS pattern could be detected.

Decreased flow through the glycolytic pathway due to treatment with TMZ in a preclinical GB model had also been detected,29 but in this instance the reduced Lac/Pyr ratio after injection of hyperpolarized Pyr was caused not by LDHA expression changes but by downregulation of the M2 isoform of the pyruvate kinase enzyme (PKM2). Furthermore, mTOR inhibition alone in a preclinical xenograft model of sarcoma also resulted in a reduced Lac/Pyr ratio after injection of hyperpolarized Pyr, 24 h after the mTOR inhibitor administration (rapamycin) and prior to any anatomic detectable changes.30

Still, there seem to be exceptions to high Lac/Pyr ratio in hyperpolarized 13C MRSI in tumours. For example, mutant isocitrate dehydrogenase 1 (IDH1) glioma models in mice31 do not produce detectable Lac after injection of hyperpolarized Pyr, due to hypermethylation of the LDHA gene promoter.32

Four recent reports have investigated the Lac/Pyr ratio (or kPL). Ravoori et al and Tee et al found that this ratio increases,33,34 whereas Park et al and Iversen et al found it to remain stable,35,36 when a variety of preclinical tumours (glioma, mammary carcinoma, ovarian, lung carcinoma) respond to therapy. In References 33, 35 and 36, the therapeutic agent used displayed anti-angiogenic or vascular disrupting activity, while in Reference 34 the drug used was an activator of PKM2. The rationale to explain this initially conflicting evidence is essentially put forward in References 33 and 36: anti-angiogenic agents will produce hypoxic regions in the tumour, causing increased glycolytic flow to maintain required ATP (adenosine triphosphate) production by the tumour cell, overriding the decreased demand of carbon precursors for cell duplication by the growth-arrested tumour cells. Thus, in the case of therapeutic drugs working through this anti-angiogenic pathway, Lac/Pyr or kPL would not be an adequate biomarker of therapeutic success and other strategies may be required to asses it. In this respect, both Park et al and Iversen et al35,36 point to a different ratio, hyperpolarized Lac/bicarbonate, as a better sensor of response to antiangiogenic agents (Supplementary Figure 4).

Take home messages. The Lac/Pyr ratio reflects the glycolytic state of tumours and could have potential for assessing tumour progression and also response to therapy, correlating with proliferation. The ratio should not be used during therapy with antiangiogenic agents as they produce hypoxic regions within tumours, and in this case the Lac/bicarbonate ratio would be more suitable.

pH changes

The fact that actively proliferating tumours display a reversed pH gradient, i.e. acidic extracellular pH (pHe) and slightly basic intracellular pH (pHi), has been known for some time.37 This is caused by active glycolysis (producing lactic acid) and oxidative metabolism (producing carbonic acid) in well perfused tumours on one hand, and active extrusion of protons and carbon dioxide/bicarbonate away from tumour cells,38 on the other. Only recently has 31P MRSI of GB patients been able to provide non-invasive images of this slightly basic pHi in proliferating GB and its changes upon transient response to therapy or in relapse. Wenger et al39 used 31P MRSI at 3 T to prove that good quality spectra can be obtained with this technique (Supplementary Figure 5) and pHi maps produced (Figure 3). In these MRSI grids, it can be shown that untreated GB has a more basic pHi than contralateral brain (mean 7.110 for tumour and mean 7.017 for contralateral brain), but also that upon transiently successful antiangiogenic therapy (bevacizumab) pHi decreases (about 7.090 at best response time), and at relapse it slightly increases again. Moreover, the region where a new tumour mass eventually appeared on relapse had mean pHi = 7.065 before therapy and before MRI signs of tumour presence, already significantly higher than contralateral (7.017); then pHi decreased, pHi = 7.044, at the time of best main mass response, and pHi increased, pHi = 7.085, at MRI detectable progression time. The higher pHi (7.065 versus 7.017) in the region where tumour relapsed later on could suggest that tumour cells were already proliferating there, but without major MRI detectable changes. In this respect pHi could predict the site of future progression in recurrent GB.

13C MRSI using hyperpolarized substances (bicarbonate) has also been used for pH imaging40 although this approach does not seem to be in use yet in the field of cancer global MR. Concomitantly, other hyperpolarized probes, such as 13C-labelled zymonic acid, have been shown to be able to produce fast and robust pHe imaging in preclinical cancer models in vivo.41,42

Take home messages. Local pH changes, essentially measured with 31P spectroscopy, can reflect cellular environment and could be useful for predicting the site of future progression in recurrent GB. In vivo measurement of pH is also possible by 13C MRS, but it has not reached the clinic.

Oncometabolites

2-hydroxyglutarate (2HG) is produced due to a neomorphic mutation,43,44 either in the moonlighting* IDH1 gene (NADP+ (nicotinamide adenine dinucleotide 2'-phosphate, oxidized form) dependent, cytoplasmic) or in IDH2 (NADP+ dependent, mitochondrial).45 2HG is defined as an oncometabolite44: in IDH1 mutants, 2HG has been reported to be mostly derived from glutamine (80%),13 and to trigger metabolic reprogramming.46,47 2HG inhibits histone demethylation48 through inhibition of α-KG-dependent dioxygenases, promotes nuclear dedifferentia- tion into a stem-cell-like state49 and downregulates choline kinase and ethanolamine kinase,50,51 among other effects. 2HG has been the subject of many studies52 by the MRS community, since IDH1 or IDH2 mutant gliomas accumulate 2HG in the millimolar range of concentration. In 2012, several publications showed that the metabolite is detectable by MRS in vivo with 3 T clinical scanners,53 and optimally when acquisition parameters are adjusted54 spectroscopic imaging can be performed55,56 to detect 2HG hot-spots and to monitor disease progression.57

Most spectral analyses are still focused on quantification of the 2HG resonances, in particular those aimed to check whether the patient is a mutant for IDH or not in a non-invasive way58,59 or to find an optimal combination of acquisition and quantification,60 and only recently are metabolomics approaches starting to be used. In Reference 61, a cohort of 47 patients was analysed with a conventional PRESS TE 35 ms SV sequence at 3 T followed by LCModel quantification and metabolomics analysis, finding that the combination of 2HG and Glx (glutamate and glutamine) values could provide better discrimination between wild-type (wt) and IDH1 mutant patients than either of them alone. In Reference 62 a small cohort of 14 glioma patients was studied by a SEMI-LASER acquisition at 7 T coupled to a non-targeted metabolomics approach, again with the goal to distinguish wt from mutant patients. Despite the pervading observations that the IDH mutation not only causes an increase in 2HG but also a change in several other metabolites, either at the initial diagnosis63,64 (Figure 4) or during assessment of response to treatment (Figure 5), the change in the metabolomic pattern seems not to be regarded with much interest in the literature. This seems surprising because 2HG is a non-invasive diagnosis and prognosis biomarker for IDH mutation,66 and it is druggable.58,65 Perhaps small cohort sizes collected by each individual study and the difficulty of integrating these data with other studies using different acquisition and processing parameters may provide an explanation for this low uptake by clinical centres. In this respect, it has been shown in ex vivo 31P HR-MAS67 of patient biopsies (five mutant IDH1 and six wt gliomas of different malignancy grades) that the phospholipid pattern differs (Supplementary Figure 6A). Recently, a larger study (n = 38) performed by Wenger et al,68 using in vivo 31P and 1H MRSI at 3 T on glioma patients of different grades, found no differences in any of the metabolites or ratios analysed by peak integration of individual resonances and univariant analysis, despite the observed trends (Supplementary Figure 6B). Wenger et al point to tumour heterogeneity and low sample size for proper stratification into grades, and to poor resolution and instrumental problems, to explain these discrepancies. In this respect, the sensitivity of 2HG detection has been shown to be dependent on voxel size (good for tumours >8 mL and bad for tumours <3.4 mL)58 on the one hand, and on the other phosphocholine (PCho) and phosphoethanolamine have been shown to be downregulated in a 2HG-dependent way.50

Mutations in the gene for succinate dehydrogenase (SDH; another moonlighting protein) cause accumulation of succinate due to impairment of its oxidation to fumarate. Succinate is nowadays regarded as an oncometabolite: its accumulation inhibits prolyl-hydroxylases in the cytosol,69 stabilizing and activating hypoxia-inducible factor (HIF)-1 alpha, and induces inflammation through this HIF-1 alpha signalling, among other roles in the cancer immune-cycle cross-talk70 (Figure 6). Succinate can be detected with MRS, and recently the SUCCES (Succinate Estimation by spectroscopy) sequence (SV, PRESS, 144 ms, 3 T) has been applied to identify carriers (about 40%) of the SDHx gene mutation among patients affected by the rare tumours pheochromocytoma or paraganglioma. Interestingly, high choline (Cho) was also reported to be associated with the succinate peak detection in patients with such a mutation (Figure 7).71

Although not yet at clinical level, mutations in fumarate hydratase are also a hallmark of some renal tumours, causing accumulation of fumarate. In addition to its role as an oncometabolite, it has also been shown that fumarate is an epigenetic modifier able to trigger the epithelial-to-mesenchymal transition.72 It had previously been shown73 that hyperpolarized fumarate can be used to monitor treatment response in murine EL-4 lymphomas through the assessment of malate production. Recently, co-polarized Pyr and fumarate have been used to monitor Lac export and necrosis in tumours.74 Fumarate has also been found to be one of the discriminant metabolites when using an untargeted metabolomics approach to assess tamoxifen treatment resistance in breast cancer cell lines.75

Take-home message. Not only oncometabolite accumulation but also the reprogrammed metabolome can be measured with MRS(I), extending the traditional single-metabolite biomarker concept.

Cho metabolism and proliferation

Abnormal Cho metabolism has been identified in different cancer types. Choline-containing compounds are involved in the biosynthesis and degra- dation of phospholipids from cell membranes. Glunde et al proposed possible causes for this abnormal metabolism,76 including changes in kinases (choline kinase-α, ethanolamine kinase-α), phospholipases (phosphatidylcholine-specific phospholipases C and D) and glycerophosphocholine (GPC) phosphodiesterases, as well as in Cho transporters. As a result of these metabolic changes, we usually expect to detect high content of PCho and tCho in actively growing tumours. In some cancer types, a low GPC content can also be observed, although it is also known that the actual tumour microenvironment can influence Cho metabolism.77

A high tCho is considered the most useful MRS(I) parameter indicating high cellular proliferation. This tCho peak consists of water-soluble choline-containing compounds, such as PCho, GPC and free Cho. In addition to this, phosphatidylcholine in cellular membranes may contribute to the tCho peak in HR-MAS ex vivo spectra at physiological recording temperature78,79 or have minor contributions to in vivo spectra in the case of small intracellular freely tumbling vesicles.80 The most relevant applications in which the tCho signal can be of help in diagnosis, prognosis or therapy response are in prostate, breast and brain cancer, and some of these applications are highlighted in the following subsections.

Prostate tumours

MRS allows the analysis of levels of choline-containing compounds, but also polyamines (PAs: spermine—Spm—and spermidine), total creatine (tCr) and citrate (Cit).81 Cit is secreted in the luminal space by normal prostate epithelial cells and accumulates at high concentrations. Levels of Cit are reduced in prostate cancer and thus may act as an in vivo biomarker to discriminate cancer from normal uninvolved prostate tissue. Regarding PAs, about 50–90% in the prostate is Spm, and they are also secreted in the luminal space by ductal cells, as is Cit. Some or all of these have been jointly used for prognosis evaluation, showing good correlation with Gleason score.82,83 Moreover, good correspondence between MRSI features and clinical outcome has been suggested,84,85 also supported by ex vivo HRMAS studies.18,86 Due to the multifocal nature of prostate cancer and its intragland heterogeneity (Supplementary Figures 3 and 7), most recent cohort studies to detect, grade or even assess response to therapy use MRSI rather than SV MRS.11,81,82,84,87-89

The information contained in the spectral pattern may vary quantitative and qualitatively according to the optimized pulse sequence and echo time used for acquisition (Figure 8).

Still, there is general consensus on the fact that metrics based on the changes in the MR-visible content of certain metabolites allow discrimination between normal tissue and prostate cancer. Thus, Cit and PAs (e.g. Spm) are high in normal tissue and choline-containing compounds (tCho) are high in cancer, while tCr does not change much. Then, different content-like ratios have been used in the past to visualize the proposed tissue type being sampled by MRSI in each volume element (Cho/Cit; [Cho + Cr (creatine)]/Cit; Cho/(Cit + PA)), although perhaps the most robust ratio, due to sometimes overlapping resonances of Cho, PA and Cr, may be (Cho + PA + Cr)/Cit.82 These content/area/peak height ratios have been transformed using diverse thresholds in predicted tissue abnormality maps or hot-spots for prostate cancer detection (Figure 9).

With respect to the clinical interest of such metrics, a retrospective study by Zakian et al84 on 262 patients at their institution concluded that prostate MRSI could help to predict outcome in radical prostatectomy patients. Additionally, Hansen et al11 found that the Cit/Cre ratio was significantly different between erythroblast transformation-specific transcriptional factor-related gene (ERG)-high and ERG-low prostate cancer patients, which could bear in vivo biomarker interest for patient progression risk stratification. Moreover, a systematic literature review of the con- tribution of MR-based methodologies to the non-invasive detection of prostate cancer concluded that MRSI provides added value on sensitivity and/or specificity values when combined with classical T2W MRI explorations.87 Still, the complexity of acquiring, post-processing and interpreting MRSI maps of patients is causing slow uptake of the use of such maps by clinical MR-based multi-parametric prostate cancer detec- tion systems (see Reference 91 for further comments on this). Using higher recording fields (7 T)89 or facilitating post-processing and display of multi-parametric datasets92 may provide a handle to improve this uptake, competing for this with the hyperpolarized 13C MRSI approach using 13C-labelled Pyr discussed above.

Breast tumours

Breast tumours present with high incidence (about 15% of all new cancer cases, according to NIH data), and early diagnosis and proper therapy response follow-up can improve patient outcome and prognosis. Breast cancer diagnosis is mostly performed using either mammography, ultrasound or MRI. However, other approaches can also provide insight into cellular processes, and their role in breast imaging is being currently evaluated. Regarding breast MRS, the spectrum of healthy breast is predominantly formed by signals from lipid protons with little contribution from water. In addition, resonances that correspond to choline-containing compounds (GPC, PCho and Cho, forming a joint peak of tCho at 3.2 ppm) are also seen.93 The Cho signal is found to be elevated in malignant breast tumours, probably due to increased tumour proliferation, and can help in distinguishing malignant from benign lesions.94 A meta-analysis performed by Baltzer and Dietzel 95 found high specificity and lower, variable sensitivity (88% and 73% respectively) of breast MRS for distinguishing lesions from uninvolved tissue. See Figure 10 for examples of breast MRSI and MRS applications.

Breast spectroscopic information can also be helpful for tumour grading, therapy monitoring and predicting response to treatment. Cho levels have been related to histologic grade and biological aggressiveness.94,96 In treated breast cancer tumours, an early decrease of Cho levels is con- sistent with tumour response and is even more sensitive than anatomic or other functional criteria.94 A recent review on in vivo and HRMAS of breast tissue metabolism by MRS provides further information on the subject.16

Brain tumours

A metabolite-ratio-derived strategy for gaining information from brain tumours by MRS(I) has been pioneered and used for some time already by Sarah Nelson's group at UCSF. These researchers used images of metabolic ‘abnormality’ at and around MRI-detected abnormal brain masses by calculating the tCho-to-N-acetylaspartate (NAA) ratio index, normalized to the same ratio in the normal contralateral brain of the same patient. This is known as CNI, where CNI values above a certain threshold would indicate presence of high-grade glioma (e.g. a z-score above 2; see References 97 and 98 for details of CNI and z-score). Other authors have used similar CNI-like indexes to simply mean direct tCho-to-NAA area ratios (Figure 11).97,98

These 'metabolic abnormality regions' have been shown to extend beyond structural MRI-defined abnormality boundaries.99-101 This is helping to better define resection margins,98 radiosurgery limits102 and malignant transformation in recurrent glioma,14 as well as to associate CNI metrics to survival after various therapeutic protocols,103,104 and to identify tumour regions at risk for progression.105

Take-home message. The Cho peak is useful to detect proliferative alterations in various tumour tissues (prostate, breast, brain), and has potential for decision making (response assessment and/or treatment planning).

MRS cancer pattern

The observation that tumours have a distinctive spectral pattern can nowadays be considered as 'old': as early as 1992 William Negendank reviewed the literature on 31P, 1H, 13C, 23Na and 19F MRS in vivo in human cancers,106 and among other conclusions stated the need for improve- ment of the diagnostic specificity and statistical analysis of multiple features, as well as trials in large populations in well-defined clinical settings. As can be noticed from previous sections, even today, pattern recognition is not much in use for the diagnostic or prognostic evaluation of cancer, with most studies focusing on single metabolites (Cho, 2HG) or particular metabolite ratios ((Cho + PA + Cr)/Cit,107 Glx/NAA,101,108) or indices (CNI), the paradigm being 2HG, a single-metabolite MRS-visible biomarker that allows clinicians to perform patient stratification and follow-up of response to therapy in carriers of the IDH mutation. However, as elaborated in Section 4.3, even in that situation other MRS-visible changes have been observed, which taken individually are non-significant. Perhaps their joint use in pattern recognition strategies could improve discrimination of the condition of interest. Furthermore, it remains to be assessed whether acquiring larger, multicentre patient cohorts, using compatible acquisition and processing protocols, could help achieve higher sensitivity and specificity (in terms of diagnostic tests) values for detection of the IDH mutation despite the low sensitivity of the MRS technique (about 1mM for 2HG and voxel sizes below 8 mL not optimal).

Recent pattern recognition studies have been dealing with two aspects: first, diagnosis, performed mainly with SV, and second, delimitation of the abnormal area, performed with MRSI. One of the main reasons for this thematic restriction is that SV MRS can address a clinically relevant question, namely the added value of MRS to MRI for brain tumour type and grade assessment.109-113 Whatever the aspect addressed, all recent studies use a 'targeted metabolomics' approach, i.e. quantification of a number of metabolites, which is set a priori, except that already mentioned by Emir and colleagues,62 where they use an untargeted approach (although in the restricted specific spectral region [1.6, 3.1] ppm).

With respect to diagnosis, the need for multicentre studies seems well established since the INTERPRET experience on preoperative brain tumour typing/grading at 1.5 T.110,114 The fact that the curated INTERPRET dataset has been made accessible to research groups allows them to develop classifiers comparing single-centre cohorts with that dataset, for example to differentiate abscesses from tumours at 3 T.115 Diagnosis of paediatric brain tumours has also been the subject of two recent works at 1.5 T on a large cohort of 90 patients109 and at 3 T in a multicentre study on 41 patients,113 to distinguish among the three main paediatric brain tumours (medulloblastoma versus pilocytic astrocytoma versus ependymoma). Despite this, single-centre studies are still reported.108

Recent studies are using pattern recognition of MRS as one of the modalities in the multiparametric assessment of tumour regions, again using a targeted metabolomics approach where pre-quantified metabolites or ratios are the input features for the classifiers. Two quantified metabolite ratios ((NAA + NAAG)/(Cr + PCho), (GPC + PCh)/(Cr + PCho)) were used in Reference 116, as well as other image features (Ktrans, Kep etc), to train a classifier to distinguish between enhancing/non enhancing tumour/non-tumour. In Reference 117 the problem addressed was the distinction between brain tumour and necrotic areas, and in Reference 118 the focus was to segment the prostate into tumour and normal tissue, providing the user with a 'nosological image'. Transformation of the metabolomic pattern information into nosological images of tissue/tumour type (Supplementary Figure 8) is an approach that was proposed 18 years ago by the group in Grenoble.119

A limitation of this approach will always be the validation of these metabolic segmentations in humans, in particular for the brain. In the case of prostate cancer, the availability of some prostatectomy specimens is an advantage and can partially help to assess the validity of the models, although a frequent problem is that the matched specimen is not available in all cases, for obvious reasons.118,120 In the brain the situation is worst, as the ground truth used for validating the metabolic segmentation must be the MRI set of images, pre-segmented by a radiologist,117,121,122 or by soft- ware.116 This means that normally the metabolic information is 'trained' to fit the anatomy, despite the fact that, in gliomas at least, it has been shown that the metabolic abnormality extends past the T2 abnormal region by a couple of centimetres.123 In this sense, the use of a semi-supervised approach (telling the system which class each spectrum belongs to, but not forcing it to classify it as one or other class) has provided robust results for prediction of response to therapy in preclinical models,124 as will be discussed in subsequent sections. During the period reviewed, methodological developments have been a primary focus: multiparametric fusion,92,121 sometimes scaling MRSI to MRI resolution by linear interpolation,116 or studying the efficacy of different implementations of non-supervised pattern recognition techniques.117,118,121,122,124,125 The problem of imbalanced classes has also been tackled with the use of AdaBoost.109 Supervised pattern recognition techniques such as support vector machines,109,115,116 linear discriminant analysis62,126 or several different algorithms,109 and classifier fusion,127 are also used in the latest literature, mainly for diagnostic questions. These methodologies are, generally too sophisticated to be put in practice by purely clinical groups, and when methodologies are tested the norm is availability of very small datasets, although there are exceptions such as Reference 113 or 109. On the other hand, groups from clinical centres tend to use simpler approaches on larger series of patients from one clinical setting. In Reference 126, Crain et al measured five peak heights with ImageJ directly over the image provided by the scanner software, to apply a linear discriminant classifier on SPSS, testing different ratio combinations, to differentiate between post-radiation effects and recurrence in gliomas, however with low success. In Reference 128, principal component analysis, a feature extraction method, is used to successfully visually distinguish one genetically different type of medulloblastoma of the four already accepted existing subtypes.129 When the multiparametric approach is tackled, methods such as logistic regression find a place, for example to predict whether the patient has prostate cancer or not,130 then restricting the MRS to the use of a ratio value (Cit/(Cho + Cr)) as one of the parameters of the predictive equation.

Take-home message. The potential of the whole spectral pattern is still underused, in particular in untargeted metabolomics approaches.

Tumours are heterogeneous tissues

MRS detects signal proportionally to the concentration of nuclei of the investigated type/molecule present (weighted by relaxation time and multiplicity effects on possible phase modulation of the signal). Simplifying a lot, we could state that MRS(I) signal intensity detected is directly proportional to the amount of the substance investigated contained in the sampled volume. In solid tumours in vivo, cancer cells constitute only a fraction of the tissue volume sampled by MR. Accordingly, between 30 and 50% of the tumour tissue (in tumours such as gliomas) can be non- cancer cells6 (mostly endothelial cells, fibroblasts and infiltrating immune cells131). Furthermore, extracellular volume and, broadly speaking, ‘inter- stitium’132 may also account for a relevant large amount of tumour tissue volume (e.g., more than 40% of tumour tissue in preclinical GL261 GB transiently responding to the TMZ therapy has been reported to be ‘acellular’133). In addition to this, dynamic changes in the 13C-labelled metabolite pattern of tumours with time (see Section 4.1 on carbon consumption by tumours) or in a steady state metabolomic pattern (see later in this section) may originate or have relevant contributions from non-cancerous cells. In this respect Guglielmetti et al134 have described an increased Lac/Pyr ratio after injection of hyperpolarized Pyr in a mouse model of multiple sclerosis with respect to control brain. The relevant point here is that Guglielmetti et al demonstrated that this increase in the Lac/Pyr ratio was due to the infiltration of the investigated brain region by the M1 subtype of proinflammatory macrophages, which are highly glycolytic cells.135 In this instance, those macrophages were shown to upregulate PDK1 (pyruvate dehydrogenase kinase 1), resulting in inhibited PDH and reduced entrance of Pyr into the TCA cycle, possibly facili- tating Pyr flow through LDH, which did not seem to be upregulated in their investigated tissue. Infiltration of tumours by innate and adaptive immune system cells is a well-known fact.9,136-138 Accordingly, the possible contribution of the metabolomic pattern of immune system cells and their changes with time/therapy to the MRS(I)-based investigation of tumours may need to be considered (see Section 4.4).

On top of the contribution of non-tumour cells to the MR-detected pattern, one additional factor to take into account is the widely recognized clonal heterogeneity of tumours,139-142 for example, in brain143 (Supplementary Figure 9), prostate141 (Supplementary Figure 7) and breast144 tumours. This will increase the variability of their metabolic pattern if large regions of interest (ROIs) are evaluated, as in SV MRS, while more relevant information with respect to this heterogeneity may be potentially sampled by multivolume MRSI approaches.

Tumour spectral pattern is also heterogeneous

Radiological and clinical guidelines are the current standards to evaluate therapy response in brain tumours, particularly through acquiring MRI and dynamic contrast-enhanced MRI data and the application of the RANO criteria. This uses 2D single slice data. However, MRSI might be a useful supplementary tool for this purpose allowing to monitor and follow-up brain tumour molecular properties and heterogeneity14,103,104,107,133,145,146 for the whole tissue (3D). Most of the time, authors focus their analysis on a few metabolites or metabolite ratios (the CNI in brain tumours, the (Cho + PA + Cr)/Cit ratio in prostate cancers), neglecting the rest of the spectral pattern, as has been discussed in Section 4.2. This has been evolving, and recently classic 'single ratio' groups have been considering additional metabolite-derived metrics: edited Lac, Cho/NAA and lipid/NAA indexes.103

According to the molecular/cellular heterogeneity described for tumours in the previous section, the spectral pattern can also be heteroge- neous through the tumour volume, reflecting differences in molecular signatures. Recent studies in human GB tend to focus on metabolite ratios in the peritumoral area.101 This is indeed true not only for a snapshot of a tumour at a given time point, but also informative in longitudinal studies, for example, to follow treatment response. This has been extensively studied in a preclinical model of GB, using pattern recognition approaches with histopathological validation.124,133,145

The spectroscopic differences between treated and untreated GL261 GB tumours were used to train a mathematical classifier that was fur- ther tested in new animals (treated and untreated), and results were validated against histopathology. Transient response producing significant survival improvement induced by TMZ was found to correlate with decreased proliferation measured by Ki67 immunostaining in histopathological slides. Prototypical spectra (source) signals were used with a semi-supervised methodology within the training set, which represented the three tissue types studied: normal brain parenchyma, GL261 tumours treated with TMZ mostly showing response or stable disease, and untreated (con- trol) GL261 tumours (i.e. actively proliferating). The changes observed in the spectral pattern of treated tumours were mainly related to mobile lipid (ML; 0.9 and 1.3 ppm) and polyunsaturated fatty acid in ML (2.8 ppm) resonances. Still, other contributions (e.g. Lac (1.3 and 4.1 ppm), glu- tamine, glutamate, alanine (3.8 ppm) and myo-inositol/glycine (3.5 ppm)) could be helping discrimination between tumour sources, although it is worth noting that the isolated analysis of chosen metabolites or their ratios did not prove useful for discriminating response, the analysis of the whole spectral pattern being the most informative and robust method of discrimination.124

The correlations between the sources and the MR spectrum of each voxel in the MRSI grids were used for calculating nosologic images. Sup- plementary Figure 10 illustrates the three groups of nosologic patterns to be recognized after training by the source methodology in the training set for the region recognized as tumour: tumours with a clear control proliferating pattern, tumours clearly responding to treatment and treated or control tumours with a partial or heterogeneous pattern of response. After the histopathological validation, the methodology was also applied to mice studied in longitudinal studies until endpoint, showing a good correlation between the nosological imaging and tumour behaviour, even predicting the outcome before evident changes were seen in their volumes.124 Furthermore, a 3D-like multislice MRSI acquisition was acquired in a new cohort of animals133 in order to assess heterogeneity along the whole tumour volume instead of a single 2D slice, and the same classifier was applied. The presence of a responding pattern was confirmed to correlate with histopathological features such as decrease of the Ki67+ deter- mined proliferation rate, while lymphocyte-like cells were also observed in the responding tumours. This led Arias-Ramos et al133 to propose a relationship between the oscillating pattern of response percentage measured in nosological images seen in GL261 GB tumours treated with TMZ and longitudinally followed until endpoint (Figure 12) and the 'immune cycle' (Supplementary Figure 11). Immune cycle-associated changes being detected by MRSI has been given additional support by other work on the GL261 GB tumour model under other therapeutic strategies (cyclophosphamide, metronomic therapy administration,147,148 and also by the duration of the immune cycle in mouse brain described in Reference 149 -6d- which is in agreement with the oscillation period recorded for the response pattern by Arias-Ramos et al.133

Take-home message. Tumours are intrinsically heterogeneous, their response is heterogeneous too, and this heterogeneity can be sampled by whole spectral pattern analysis of MRS(I). There is a non-negligible contribution from non-tumoral cells such as tumour- associated macrophages.

What are the limitations of MRS(I)?

Some of the main disadvantages or limitations of MRS (mainly MRSI) are longer acquisition times needed for data collection, compared with classic structural MRI, lack of adequate signal-to-noise ratio (SNR), sometimes improper water/lipid signal suppression and limitations in spatial coverage. Moreover, it is worth noting that an MRS(I) exploration is equivalent to a snapshot of a given system, and most of the in vivo processes, mainly the metabolic ones, are dynamic. This means that some processes can be either missed or improperly sampled, because in long explorations the final output will be an average of the processes taking place during the overall acquisition time.

The range of metabolites that can be studied in tumours is limited

MRS (in either its single or multi-voxel modality, respectively SV-MRS or MRSI) has the ability to detect changes in the relative content of metabolites, even allowing the calculation of absolute concentrations. Still, only small and/or mobile molecules, in the millimolar concentration range, are directly observed in an in vivo MR spectrum. This is extremely low as compared with tissue water (about 55 M). Therefore, proper water suppression (and also lipid suppression in the case of tumour surrounded by adipose tissue, e.g. subcutaneous fat, scalp lipids) is required for confident metabolite observation and quantitation. The biological significance of the major compounds found in tissues, for example in brain spectra and tumours, is reviewed in References10,17 and.150-152 Other minority substances are hardly detected due to either extremely small or overlapping signals, although spectral editing may allow their observation and quantification.153

The resolution achieved is usually lower than MRI resolution

As the concentrations of the MRS-detected metabolites are much lower than that of water, larger voxel sizes are needed to detect enough signal for MRS(I) with respect to MRI. This prevents MRSI from providing comparable resolution to MRI (although further post-processing, i.e. interpo- lation, can partially address this limitation). The lower spatial resolution of MRSI compared with anatomical imaging makes consideration of the contribution of the spatial point spread function (signal bleeding into the surrounding voxels, producing a blurring effect154), proportionally more relevant than for MRI.

3.3.3 | There is important sensitivity to magnetic field variation

Another important point is the MRSI sensitivity to magnetic field inhomogeneity across the volume of interest (VOI), which may require avoiding anatomical regions prone to present strong magnetic field inhomogeneity such as tissue-bone or tissue-air interfaces in order to avoid line broadening and spectral artifacts. This is one of the reasons why MRSI has been most successful in brain tumour acquisitions: more favourable field homogeneity conditions and sensitive signal detection due to the use of surface coil arrays close to the volume being sampled. Accordingly, MRSI has been extensively applied for diagnosis and treatment follow-up of brain tumours. Regarding prostate tumours, MRSI acquisition is usu- ally performed with an endorectal coil for signal reception, to achieve good SNRs. However, it also implies longer time needed for preparation, as well as patient discomfort. Tayari et al91 describe MRSI acquisition approaches without an endorectal coil obtaining good quality MRSI data, which would probably contribute to increasing its incorporation in clinical pipelines for prostate cancer diagnosis and follow-up in the future. Finally, regarding the breast, the relevant magnetic field inhomogeneities observed, as well as the small water peak in adipose tissue, make shimming quite challenging in these anatomical locations.

Conclusions

Regarding cancer metabolomics analysis, MRSI should be the standard choice for in vivo (pre) clinical MRSI due to its ability to provide spatially resolved information, and consequently details of relevance with respect to tumour tissue heterogeneity, which are not provided by SV MRS. However, this is restricted to applications in which limited volume coverage and spatial resolution with respect to MRI/MRS are acceptable, and also where the achievable homogeneity of the magnetic field is not an issue. SV MRS will remain an important tool for evaluating metabolite content in regions where magnetic field inhomogeneity degrades spectral quality in MRSI or when single biomarker detection may be of interest (2HG detection in LGG brain tumours). Although most clinical studies focus into 1H-MRS(I), there are different studies using 13C and 31P, which could be also of help either in grading or therapy response assessment by monitoring carbon consumption and local pH changes. The study of single metabolite biomarkers (e.g. Cho, 2HG) has also shown its potential in the diagnostic and prognostic assessment of tumours. However, the study of single metabolites or metabolite ratios offers a restricted picture of the metabolic reprogramming that occurs in tumours, which is being acknowledged in recent literature and could be better tackled by a pattern recognition approach. Recent pattern recognition studies are primarily focused on methodological developments rather than multicentre validation of preclinical or clinical study findings based on small one-centre cohorts. Additional steps toward simplification and standardization of processing files from different vendors would probably be needed in this sense, as well as familiarization of clinicians and researchers with pattern recognition tools. Novel dynamic metabolic approaches such as using hyperpolarized substrates will probably have considerable impact on future applications of MRSI and technology development, pro- vided that large animal/patient cohorts are explored at more than one site with comparable data acquisition protocols.

References

1. Wang J, Weygand J, Hwang KP, et al. Magnetic resonance imaging of glucose uptake and metabolism in patients with head and neck cancer. Sci Rep.
2016;6:30618.
2. Goldenberg JM, Pagel MD. Assessments of tumor metabolism with CEST MRI. NMR Biomed. 2018;e3943.
3. Dietz C, Ehret F, Palmas F, et al. Applications of high-resolution magic angle spinning MRS in biomedical studies II—human diseases. NMR Biomed. 2017;30(11):e3784.
4. Hanahan D, Weinberg RA. Hallmarks of cancer: the next generation. Cell. 2011;144(5):646-674.
5. Pavlova NN, Thompson CB. The emerging hallmarks of cancer metabolism. Cell Metab. 2016;23(1):27-47.
6. Hambardzumyan D, Gutmann DH, Kettenmann H. The role of microglia and macrophages in glioma maintenance and progression. Nat Neurosci.
2016;19(1):20-27.
7. Esparza-Lopez J, Escobar-Arriaga E, Soto-Germes S, Ibarra-Sanchez MJ. Breast cancer intra-tumor heterogeneity: one tumor, different entities. Rev Invest Clin. 2017;69(2):66-76.
8. Chiarugi P, Paoli P, Cirri P. Tumor microenvironment and metabolism in prostate cancer. Semin Oncol. 2014;41(2):267-280.
9. Glass R, Synowitz M. CNS macrophages and peripheral myeloid cells in brain tumours. Acta Neuropathol. 2014;128(3):347-362.
10. Kostidis S, Addie RD, Morreau H, Mayboroda OA, Giera M. Quantitative NMR analysis of intra- and extracellular metabolism of mammalian cells: a tutorial. Anal Chim Acta. 2017;980:1-24.
11. Hansen AF, Sandsmark E, Rye MB, et al. Presence of TMPRSS2-ERG is associated with alterations of the metabolic profile in human prostate cancer.
Oncotarget. 2016;7(27):42071-42085.
12. Wang AS, Lodi A, Rivera LB, et al. HR-MAS MRS of the pancreas reveals reduced lipid and elevated lactate and taurine associated with early pancreatic cancer. NMR Biomed.
2014;27(11):1361-1370.Izquierdo-Garcia JL, Viswanath P, Eriksson P, et al. IDH1 mutation induces reprogramming of pyruvate metabolism. Cancer Res.
2015;75(15):2999-3009.
13. Jalbert LE, Elkhaled A, Phillips JJ, et al. Metabolic profiling of IDH mutation and malignant progression in infiltrating glioma. Sci Rep. 2017;7:44792.
14. Vandergrift LA, Decelle EA, Kurth J, et al. Metabolomic prediction of human prostate cancer aggressiveness: magnetic resonance spectroscopy of his- tologically benign tissue. Sci Rep. 2018;8(1):4997.
15. Jagannathan NR, Sharma U. Breast tissue metabolism by magnetic resonance spectroscopy. Metabolites. 2017;7(2):pii E25.
16. Madhu B, Jauhiainen A, McGuire S, Griffiths JR. Exploration of human brain tumour metabolism using pairwise metabolite-metabolite correlation analysis (MMCA) of HR-MAS 1H NMR spectra. PLoS ONE. 2017;12(10):e0185980.
17. Madhu B, Shaw GL, Warren AY, Neal DE, Griffiths JR. Response of Degarelix treatment in human prostate cancer monitored by HR-MAS 1H NMR spectroscopy. Metabolomics. 2016;12:120.
18. Fuss TL, Cheng LL. Evaluation of cancer metabolomics using ex vivo high resolution magic angle spinning (HRMAS) magnetic resonance spectroscopy (MRS). Metabolites. 2016;6(1):pii E11.

19. Li C, Zhang G, Zhao L, Ma Z, Chen H. Metabolic reprogramming in cancer cells: glycolysis, glutaminolysis, and Bcl-2 proteins as novel therapeutic tar- gets for cancer. World J Surg Oncol. 2016;14(1):15.
20. Dang CV. Links between metabolism and cancer. Genes Dev. 2012;26(9):877-890.
21. Vander Heiden MG, Cantley LC, Thompson CB. Understanding the Warburg effect: the metabolic requirements of cell proliferation. Science. 2009;324(5930):1029-1033.
22. Serrao EM, Kettunen MI, Rodrigues TB, et al. MRI with hyperpolarised [1-13C] pyruvate detects advanced pancreatic preneoplasia prior to invasive disease in a mouse model. Gut. 2016;65(3):465-475.
23. Najac C, Ronen SM. MR molecular imaging of brain cancer metabolism using hyperpolarized 13C magnetic resonance spectroscopy. Top Magn Reson Imaging. 2016;25(5):187-196.
24. Chen HY, Larson PEZ, Bok RA, et al. Assessing prostate cancer aggressiveness with hyperpolarized dual-agent 3d dynamic imaging of metabolism and perfusion. Cancer Res. 2017;77(12):3207-3216.
25. Nelson SJ, Kurhanewicz J, Vigneron DB, et al. Metabolic imaging of patients with prostate cancer using hyperpolarized [1-13C]pyruvate. Sci Transl Med. 2013;5(198). 198ra108
26. Aggarwal R, Vigneron DB, Kurhanewicz J. Hyperpolarized 1-[13C]-pyruvate magnetic resonance imaging detects an early metabolic response to andro- gen ablation therapy in prostate cancer. Eur Urol. 2017;72(6):1028-1029.
27. Radoul M, Chaumeil MM, Eriksson P, Wang AS, Phillips JJ, Ronen SM. MR studies of glioblastoma models treated with dual PI3K/mTOR inhibitor and temozolomide: metabolic changes are associated with enhanced survival. Mol Cancer Ther. 2016;15(5):1113-1122.
28. Park I, Mukherjee J, Ito M, et al. Changes in pyruvate metabolism detected by magnetic resonance imaging are linked to DNA damage and serve as a sensor of temozolomide response in glioblastoma cells. Cancer Res. 2014;74(23):7115-7124.
29. Di Gialleonardo V, Aldeborgh HN, Miloushev V, et al. Multinuclear NMR and MRI reveal an early metabolic response to mTOR inhibition in sarcoma. Cancer Res. 2017;77(11):3113-3120.
30. Chaumeil MM, Radoul M, Najac C, et al. Hyperpolarized 13C MR imaging detects no lactate production in mutant IDH1 gliomas: implications for diagnosis and response monitoring. NeuroImage Clin. 2016;12:180-189.
31. Chesnelong C, Chaumeil MM, Blough MD, et al. Lactate dehydrogenase A silencing in IDH mutant gliomas. Neuro-Oncology. 2014;16(5):686-695.
32. Ravoori MK, Singh SP, Lee J, Bankson JA, Kundra V. In vivo assessment of ovarian tumor response to tyrosine kinase inhibitor pazopanib by using hyperpolarized 13C-pyruvate MR spectroscopy and 18F-FDG PET/CT imaging in a mouse model. Radiology. 2017;285(3):830-838.
33. Tee SS, Park JM, Hurd RE, et al. PKM2 activation sensitizes cancer cells to growth inhibition by 2-deoxy-D-glucose. Oncotarget. 2017;8(53):90959-90968.
34. Park JM, Spielman DM, Josan S, et al. Hyperpolarized 13C-lactate to 13C-bicarbonate ratio as a biomarker for monitoring the acute response of anti- vascular endothelial growth factor (anti-VEGF) treatment. NMR Biomed. 2016;29(5):650-659.
35. Iversen AB, Busk M, Bertelsen LB, et al. The potential of hyperpolarized 13C magnetic resonance spectroscopy to monitor the effect of combretastatin based vascular disrupting agents. Acta Oncol. 2017;56(11):1626-1633.
36. Griffiths JR. Are cancer cells acidic? Br J Cancer. 1991;64(3):425-427.

37. Stubbs M, McSheehy PM, Griffiths JR, Bashford CL. Causes and consequences of tumour acidity and implications for treatment. Mol Med Today.
2000;6(1):15-19.
38. Wenger KJ, Hattingen E, Franz K, Steinbach JP, Bahr O, Pilatus U. Intracellular pH measured by 31P-MR-spectroscopy might predict site of progression in recurrent glioblastoma under antiangiogenic therapy. J Magn Reson Imaging. 2017;46(4):1200-1208.
39. Gallagher FA, Kettunen MI, Day SE, et al. Magnetic resonance imaging of pH in vivo using hyperpolarized 13C-labelled bicarbonate. Nature.
2008;453(7197):940-943.
40. Duwel S, Hundshammer C, Gersch M, et al. Imaging of pH in vivo using hyperpolarized 13C-labelled zymonic acid. Nat Commun. 2017;8:15126.
41. Hundshammer C, Duwel S, Kocher SS, et al. Deuteration of hyperpolarized 13C-labeled zymonic acid enables sensitivity-enhanced dynamic MRI of pH.
ChemPhysChem. 2017;18(18):2422-2425.
42. Moore S, Järvelin AI, Davis I, Bond GL, Castello A. Expanding horizons: new roles for non-canonical RNA-binding proteins in cancer. Curr Opin Gen Dev.
2018;48:112-120.
43. Yan H, Parsons DW, Jin G, et al. IDH1 and IDH2 mutations in gliomas. N Engl J Med.
2009;360(8):765-773.
44. Zhao S, Lin Y, Xu W, et al. Glioma-derived mutations in IDH1 dominantly inhibit IDH1 catalytic activity and induce HIF-1alpha. Science.
2009;324(5924):261-265.
45. Viswanath P, Chaumeil MM, Ronen SM. Molecular imaging of metabolic reprograming in mutant IDH cells. Front Oncol. 2016;6(60). https://doi.org/ 10.3389/fonc.2016.00060Izquierdo-Garcia JL, Viswanath P, Eriksson P, et al. Metabolic reprogramming in mutant IDH1 glioma cells. PLoS ONE. 2015;10(2):e0118781.
46. Lu C, Ward PS, Kapoor GS, et al. IDH mutation impairs histone demethylation and results in a block to cell differentiation. Nature.
2012;483(7390):474-478.
47. Menendez Javier A, Corominas-Faja B, Cuyàs E, et al. Oncometabolic nuclear reprogramming of cancer stemness. Stem Cell Rep. 2016;6(3):273-283.
48. Viswanath P, Radoul M, Izquierdo-Garcia JL, et al. Mutant IDH1 gliomas downregulate phosphocholine and phosphoethanolamine synthesis in a 2-hydroxyglutarate-dependent manner. Cancer Metab. 2018;6:3.
49. Viswanath P, Radoul M, Izquierdo-Garcia JL, et al. 2-hydroxyglutarate-mediated autophagy of the endoplasmic reticulum leads to an unusual down- regulation of phospholipid biosynthesis in mutant IDH1 gliomas. Cancer Res. 2018;78(9):2290-2304.
50. Kickingereder P, Andronesi OC. Radiomics, metabolic, and molecular MRI for brain tumors. Semin Neurol. 2018;38(1):32-40.
51. Pope WB, Prins RM, Albert Thomas M, et al. Non-invasive detection of 2-hydroxyglutarate and other metabolites in IDH1 mutant glioma patients using magnetic resonance spectroscopy. J Neurooncol. 2011;107(1):197-205.
52. An Z, Tiwari V, Ganji SK, et al. Echo-planar spectroscopic imaging with dual-readout alternated gradients (DRAG-EPSI) at 7 T: application for 2-hydroxyglutarate imaging in glioma patients. Magn Reson Med. 2018;79(4):1851-1861.
53. Choi C, Ganji SK, DeBerardinis RJ, et al. 2-hydroxyglutarate detection by magnetic resonance spectroscopy in IDH-mutated patients with gliomas. Nat Med. 2012;18(4):624-629.

54. Andronesi OC, Kim GS, Gerstner E, et al. Detection of 2-hydroxyglutarate in IDH-mutated glioma patients by in vivo spectral-editing and 2D corre- lation magnetic resonance spectroscopy. Sci Transl Med. 2012, 4;116. 116ra114
55. Choi C, Raisanen JM, Ganji SK, et al. Prospective longitudinal analysis of 2-hydroxyglutarate magnetic resonance spectroscopy identifies broad clinical utility for the management of patients with IDH-mutant glioma. J Clin Oncol. 2016;34(33):4030-4039.
56. de la Fuente MI, Young RJ, Rubel J, et al. Integration of 2-hydroxyglutarate-proton magnetic resonance spectroscopy into clinical practice for disease monitoring in isocitrate dehydrogenase-mutant glioma. Neuro-Oncology. 2016;18(2):283-290.
57. Branzoli F, Di Stefano AL, Capelle L, et al. Highly specific determination of IDH status using edited in vivo magnetic resonance spectroscopy. Neuro- Oncology. 2018;20(7):907-916.
58. Berrington A, Voets NL, Larkin SJ, et al. A comparison of 2-hydroxyglutarate detection at 3 and 7 T with long-TE semi-LASER. NMR Biomed.
2018;31(3):e3886.
59. Nagashima H, Tanaka K, Sasayama T, et al. Diagnostic value of glutamate with 2-hydroxyglutarate in magnetic resonance spectroscopy for IDH1 mutant glioma. Neuro-Oncology. 2016;18(11):1559-1568.
60. Emir UE, Larkin SJ, de Pennington N, et al. Noninvasive quantification of 2-hydroxyglutarate in human gliomas with IDH1 and IDH2 mutations. Cancer Res. 2016;76(1):43-49.
61. Natsumeda M, Igarashi H, Nomura T, et al. Accumulation of 2-hydroxyglutarate in gliomas correlates with survival: a study by 3.0-tesla magnetic res- onance spectroscopy. Acta Neuropathol Commun. 2014;2:158.
62. Natsumeda M, Motohashi K, Igarashi H, et al. Reliable diagnosis of IDH-mutant glioblastoma by 2-hydroxyglutarate detection: a study by 3-T magnetic resonance spectroscopy. Neurosurg Rev. 2018;41(2):641-647.
63. Andronesi OC, Arrillaga-Romany IC, Ly KI, et al. Pharmacodynamics of mutant-IDH1 inhibitors in glioma patients probed by in vivo 3D MRS imaging of 2-hydroxyglutarate. Nat Commun. 2018;9(1):1474.
64. Leather T, Jenkinson MD, Das K, Poptani H. Magnetic resonance spectroscopy for detection of 2-hydroxyglutarate as a biomarker for IDH mutation in gliomas. Metabolites. 2017;7(2):E29.
65. Esmaeili M, Hamans BC, Navis AC, et al. IDH1 R132H mutation generates a distinct phospholipid metabolite profile in glioma. Cancer Res.
2014;74(17):4898-4907.
66. Wenger KJ, Hattingen E, Franz K, Steinbach J, Bahr O, Pilatus U. In vivo metabolic profiles as determined by 31P and short TE 1H MR-spectroscopy: no difference between patients with IDH wildtype and IDH mutant gliomas. Clin Neuroradiol. 2017. https://doi.org/10.1007/s00062-017-0630-8
67. Selak MA, Armour SM, MacKenzie ED, et al. Succinate links TCA cycle dysfunction to oncogenesis by inhibiting HIF-alpha prolyl hydroxylase. Cancer Cell. 2005;7(1):77-85.
68. Jiang S, Yan W. Succinate in the cancer-immune cycle. Cancer Lett. 2017;390:45-47.
69. Lussey-Lepoutre C, Bellucci A, Morin A, et al. In vivo detection of succinate by magnetic resonance spectroscopy as a hallmark of SDHx mutations in paraganglioma. Clin Cancer Res. 2016;22(5):1120-1129.
70. Sciacovelli M, Goncalves E, Johnson TI, et al. Fumarate is an epigenetic modifier that elicits epithelial-to-mesenchymal transition. Nature.
2016;537(7621):544-547.

71. Gallagher FA, Kettunen MI, Hu DE, et al. Production of hyperpolarized [1,4-13C2] malate from [1,4-13C2] fumarate is a marker of cell necrosis and treatment response in tumors. Proc Natl Acad Sci U S A. 2009;106(47):19801-19806.
72. Feuerecker B, Durst M, Michalik M, et al. Hyperpolarized 13C diffusion MRS of co-polarized pyruvate and fumarate to measure lactate export and necrosis. J Cancer. 2017;8(15):3078-3085.
73. Kim HS, Tian L, Kim H, Moon WK. Investigation of discriminant metabolites in tamoxifen-resistant and choline kinase-alpha-downregulated breast cancer cells using 1H-nuclear magnetic resonance spectroscopy. PLoS ONE. 2017;12(6):e0179773.
74. Glunde K, Penet MF, Jiang L, Jacobs MA, Bhujwalla ZM. Choline metabolism-based molecular diagnosis of cancer: an update. Exp Rev Mol Diagn.
2015;15(6):735-747.
75. Glunde K, Bhujwalla ZM, Ronen SM. Choline metabolism in malignant transformation. Nat Rev Cancer. 2011;11(12):835-848.
76. Jimenez-Xarrie E, Davila M, Gil-Perotin S, et al. In vivo and ex vivo magnetic resonance spectroscopy of the infarct and the subventricular zone in experimental stroke. J Cereb Blood Flow Metab. 2015;35(5):828-834.
77. Davila M, Candiota AP, Pumarola M, Arus C. Minimization of spectral pattern changes during HRMAS experiments at 37 degrees celsius by prior focused microwave irradiation. Magn Reson Mater Phys Biol Med. 2012;25(5):401-410.
78. artin-Sitjar J, Delgado-Goni T, Cabanas ME, Tzen J, Arus C. Influence of the spinning rate in the HR-MAS pattern of mobile lipids in C6 glioma cells and in artificial oil bodies. Magn Reson Mater Phys Biol Med. 2012;25(6):487-496.
79. Tayari N, Heerschap A, Scheenen TWJ, Kobus T. In vivo MR spectroscopic imaging of the prostate, from application to interpretation. Anal Biochem.
2017;529:158-170.
80. Weis J, von Below C, Tolf A, et al. Quantification of metabolite concentrations in benign and malignant prostate tissues using 3D proton MR spectro- scopic imaging. J Magn Reson Imaging. 2017;45(4):1232-1240.
81. Dwivedi DK, Kumar R, Bora GS, et al. Stratification of the aggressiveness of prostate cancer using pre-biopsy multiparametric MRI (mpMRI). NMR Biomed. 2016;29(3):232-238.
82. Zakian KL, Hatfield W, Aras O, et al. Prostate MRSI predicts outcome in radical prostatectomy patients. Magn Reson Imaging. 2016;34(5):674-681.
83. Zakian KL, Hricak H, Ishill N, et al. An exploratory study of endorectal magnetic resonance imaging and spectroscopy of the prostate as preoperative predictive biomarkers of biochemical relapse after radical prostatectomy. J Urol. 2010;184(6):2320-2327.
84. Braadland PR, Giskeodegard G, Sandsmark E, et al. Ex vivo metabolic fingerprinting identifies biomarkers predictive of prostate cancer recurrence following radical prostatectomy. Br J Cancer. 2017;117(11):1656-1664.
85. Fusco R, Sansone M, Granata V, Setola SV, Petrillo A. A systematic review on multiparametric MR imaging in prostate cancer detection. Infect Agent Cancer. 2017;12:57.
86. Testa C, Pultrone C, Manners DN, Schiavina R, Lodi R. Metabolic imaging in prostate cancer: where we are. Front Oncol. 2016;6:225.
87. Lagemaat MW, Breukels V, Vos EK, et al. 1H MR spectroscopic imaging of the prostate at 7 T using spectral-spatial pulses. Magn Reson Med.
2016;75(3):933-945.
88. Kobus T, Wright AJ, Scheenen TW, Heerschap A. Mapping of prostate cancer by 1H MRSI. NMR Biomed. 2014;27(1):39-52.

89. Tayari N, Steinseifer IK, Selnaes KM, Bathen TF, Maas MC, Heerschap A. High-quality 3-dimensional 1H magnetic resonance spectroscopic imaging of the prostate without endorectal receive coil using a semi-LASER sequence. Invest Radiol. 2017;52(10):640-646.
90. Lemaitre G, Marti R, Rastgoo M, Meriaudeau F. Computer-aided detection for prostate cancer detection based on multi-parametric magnetic reso- nance imaging. Proc IEEE Eng Med Biol Soc. 2017;2017:3138-3141.
91. Tafreshi NK, Kumar V, Morse DL, Gatenby RA. Molecular and functional imaging of breast cancer. Cancer Control. 2010;17(3):143-155.
92. Martin Noguerol T, Sanchez-Gonzalez J, Martinez Barbero JP, Garcia-Figueiras R, Baleato-Gonzalez S, Luna A. Clinical imaging of tumor metabolism with 1H magnetic resonance spectroscopy. Magn Reson Imaging Clin N Am. 2016;24(1):57-86.
93. Baltzer PA, Dietzel M. Breast lesions: diagnosis by using proton MR spectroscopy at 1.5 and 3.0 T—systematic review and meta-analysis. Radiology. 2013;267(3):735-746.
94. Shin HJ, Baek H-M, Cha JH, Kim HH. Evaluation of breast cancer using proton MR spectroscopy: total choline peak integral and signal-to-noise ratio as prognostic indicators. Am J Roentgenol. 2012;198(5):W488-W497.
95. Guo J, Yao C, Chen H, et al. The relationship between Cho/NAA and glioma metabolism: implementation for margin delineation of cerebral gliomas. Acta Neurochir. 2012;154(8):1361-1370.
96. Zhang J, Zhuang DX, Yao CJ, et al. Metabolic approach for tumor delineation in glioma surgery: 3D MR spectroscopy image-guided resection. J Neurosurg. 2016;124(6):1585-1593.
97. McKnight TR, Noworolski SM, Vigneron DB, Nelson SJ. An automated technique for the quantitative assessment of 3D-MRSI data from patients with glioma. J Magn Reson Imaging. 2001;13(2):167-177.
98. Ganslandt O, Stadlbauer A, Fahlbusch R, et al. Proton magnetic resonance spectroscopic imaging integrated into image-guided surgery: correlation to standard magnetic resonance imaging and tumor cell density. Neurosurgery. 2005;56(4):291-298.
99. Pedrosa de Barros N, Meier R, Pletscher M, et al. On the relation between MR spectroscopy features and the distance to MRI-visible solid tumor in GBM patients. Magn Reson Med. 2018;80(6):2339-2355.
100. Shen G, Xu L, Xu M, Geng M, Tan Y, Li F. 1H-MR spectroscopy guided gamma knife radiosurgery for treatment of glioma. Turk Neurosurg. 2012;22(6):690-694.
101. Nelson SJ, Kadambi AK, Park I, et al. Association of early changes in 1H MRSI parameters with survival for patients with newly diagnosed glioblastoma receiving a multimodality treatment regimen. Neuro-Oncology. 2017;19(3):430-439.
102. Nelson SJ, Li Y, Lupo JM, et al. Serial analysis of 3D H-1 MRSI for patients with newly diagnosed GBM treated with combination therapy that includes bevacizumab. J Neurooncol. 2016;130(1):171-179.
103. Anwar M, Molinaro AM, Morin O, et al. Identifying voxels at risk for progression in glioblastoma based on dosimetry, physiologic and metabolic MRI. Radiat Res. 2017;188(3):303-313.
104. Negendank W. Studies of human tumors by MRS: a review. NMR Biomed. 1992;5(5):303-324.

105. Ratai E-M, Zhang Z, Fink J, et al. ACRIN 6684: multicenter, phase II assessment of tumor hypoxia in newly diagnosed glioblastoma using magnetic resonance spectroscopy. PLoS ONE. 2018;13(6):e0198548.
106. Kaur T, Saini BS, Gupta S. An optimal spectroscopic feature fusion strategy for MR brain tumor classification using Fisher criteria and parameter-free BAT optimization algorithm. Biocybern Biomed Eng. 2018;38(2):409-424.
107. Zarinabad N, Wilson M, Gill SK, Manias KA, Davies NP, Peet AC. Multiclass imbalance learning: improving classification of pediatric brain tumors from magnetic resonance spectroscopy. Magn Reson Med. 2017;77(6):2114-2124.
108. Julia-Sape M, Griffiths JR, Tate AR, et al. Classification of brain tumours from MR spectra: the INTERPRET collaboration and its outcomes. NMR Biomed. 2015;28(12):1772-1787.
109. Julià-Sapé M, Coronel I, Majós C, et al. Prospective diagnostic performance evaluation of single-voxel 1H MRS for typing and grading of brain tumours.
NMR Biomed. 2012;24(4):661-673.
110. Majos C, Aguilera C, Alonso J, et al. Proton MR spectroscopy improves discrimination between tumor and pseudotumoral lesion in solid brain masses.
Am J Neuroradiol. 2009;30(3):544-551.Zarinabad N, Abernethy LJ, Avula S, et al. Application of pattern recognition techniques for classification of pediatric brain tumors by in vivo 3 T
1H-MR spectroscopy—a multi-center study. Magn Reson Med. 2018;79(4):2359-2366.
111. Tate AR, Underwood J, Acosta DM, et al. Development of a decision support system for diagnosis and grading of brain tumours using in vivo magnetic resonance single voxel spectra. NMR Biomed. 2006;19(4):411-434.
112. Vieira BH, Santos AC, Salmon CEG. Pattern recognition of abscesses and brain tumors through MR spectroscopy: comparison of experimental condi- tions and radiological findings. Res Biomed Eng. 2017;33:185-194.
113. Blumenthal DT, Artzi M, Liberman G, Bokstein F, Aizenstein O, Ben BD. Classification of high-grade glioma into tumor and nontumor components using support vector machine. Am J Neuroradiol. 2017;38(5):908-914.
114. Sauwen N, Sima DM, Cauter SV, et al. Hierarchical non-negative matrix factorization to characterize brain tumor heterogeneity using multi-parametric MRI. NMR Biomed. 2015;28(12):1599-1624.
115. Laudadio T, Croitor Sava AR, Sima DM, et al. Hierarchical non-negative matrix factorization applied to three-dimensional 3 T MRSI data for automatic tissue characterization of the prostate. NMR Biomed. 2016;29(6):751-758.
116. De Edelenyi FS, Rubin C, Esteve F, et al. A new approach for analyzing proton magnetic resonance spectroscopic images of brain tumors: nosologic images. Nat Med. 2000;6(11):1287-1289.
117. De Visschere PJ, Vral A, Perletti G, et al. Multiparametric magnetic resonance imaging characteristics of normal, benign and malignant conditions in the prostate. Eur Radiol. 2017;27(5):2095-2109.
118. Li Y, Liu X, Wei F, et al. An advanced MRI and MRSI data fusion scheme for enhancing unsupervised brain tumor differentiation. Comput Biol Med.
2017;81:121-129.
119. Bharath HN, Sima DM, Sauwen N, Himmelreich U, De Lathauwer L, Van Huffel S. Nonnegative canonical polyadic decomposition for tissue-type differentiation in gliomas. IEEE J Biomed Health Inform. 2017;21(4):1124-1132.
120. Pirzkall A, McKnight TR, Graves EE, et al. MR-spectroscopy guided target delineation for high-grade gliomas. Int J Radiat Oncol Biol Phys.

2001;50(4):915-928.
121. Delgado-Goni T, Ortega-Martorell S, Ciezka M, et al. MRSI-based molecular imaging of therapy response to temozolomide in preclinical glioblastoma using source analysis. NMR Biomed. 2016;29(6):732-743.
122. Mocioiu V, de Barros NMP, Ortega-Martorell S, et al. A machine learning pipeline for supporting differentiation of glioblastomas from single brain metastases. In: ESANN 2016 Proceedings: European Symposium on Artificial Neural Networks, Computational Intelligence and Machine Learning Bruges (Belgium), 27–29 April 2016.2016:247–252. https://www.elen.ucl.ac.be/esann/proceedings/papers.php?ann=2016
123. Crain ID, Elias PS, Chapple K, Scheck AC, Karis JP, Preul MC. Improving the utility of 1H-MRS for the differentiation of glioma recurrence from radiation necrosis. J Neurooncol. 2017;133(1):97-105.
124. Beigi M, Ghasemi K, Mirzaghavami P, Khanmohammadi M, SalighehRad H. Malignancy probability map as a novel imaging biomarker to predict malignancy distribution: employing MRS in GBM patients. J Neurooncol. 2018;138(3):619-625.
125. Bluml S, Margol AS, Sposto R, et al. Molecular subgroups of medulloblastoma identification using noninvasive magnetic resonance spectroscopy.
Neuro-Oncology. 2016;18(1):126-131.
126. Northcott PA, Korshunov A, Witt H, et al. Medulloblastoma comprises four distinct molecular variants. J Clin Oncol. 2011;29(11):1408-1414.
127. Dwivedi DK, Kumar R, Dwivedi AK, et al. Prebiopsy multiparametric MRI-based risk score for predicting prostate cancer in biopsy-naive men with prostate-specific antigen between 4–10 ng/mL. J Magn Reson Imaging. 2018;47(5):1227-1236.
128. Egeblad M, Nakasone ES, Werb Z. Tumors as organs: complex tissues that interface with the entire organism. Dev Cell. 2010;18(6):884-901.
129. Benias PC, Wells RG, Sackey-Aboagye B, et al. Structure and distribution of an unrecognized interstitium in human tissues. Sci Rep. 2018;8(1):4947.
130. Arias-Ramos N, Ferrer-Font L, Lope-Piedrafita S, et al. Metabolomics of therapy response in preclinical glioblastoma: a multi-slice MRSI-based volu- metric analysis for noninvasive assessment of temozolomide treatment. Metabolites. 2017;7(2):E20.
131. Guglielmetti C, Najac C, Didonna A, Van der Linden A, Ronen SM, Chaumeil MM. Hyperpolarized 13C MR metabolic imaging can detect neuroinflam- mation in vivo in a multiple sclerosis murine model. Proc Natl Acad Sci U S A. 2017;114(33):E6982-E6991.
132. Langston PK, Shibata M, Horng T. Metabolism supports macrophage activation. Front Immunol. 2017;8:61.
133. Morantz RA, Wood GW, Foster M, Clark M, Gollahon K. Macrophages in experimental and human brain tumors. Part 2: studies of the macrophage content of human brain tumors. J Neurosurg. 1979;50(3):305-311.
134. Lapa C, Linsenmann T, Luckerath K, et al. Tumor-associated macrophages in glioblastoma multiforme—a suitable target for somatostatin receptor- based imaging and therapy? PLoS ONE. 2015;10(3):e0122269.
135. Domingues P, Gonzalez-Tablas M, Otero A, et al. Tumor infiltrating immune cells in gliomas and meningiomas. Brain Behav Immun. 2016;53:1-15.
136. Soeda A, Hara A, Kunisada T, Yoshimura S, Iwama T, Park DM. The evidence of glioblastoma heterogeneity. Sci Rep. 2015;5:7979.
137. Bi WL, Zhang M, Wu WW, Mei Y, Dunn IF. Meningioma genomics: diagnostic, prognostic, and therapeutic applications. Front Surg. 2016;3:40.

138. Cyll K, Ersvaer E, Vlatkovic L, et al. Tumour heterogeneity poses a significant challenge to cancer biomarker research. Br J Cancer. 2017;117(3):367-375.
139. Polyak K. Heterogeneity in breast cancer. J Clin Invest. 2011;121(10):3786-3788.
140. Sottoriva A, Spiteri I, Piccirillo SG, et al. Intratumor heterogeneity in human glioblastoma reflects cancer evolutionary dynamics. Proc Natl Acad Sci U S A. 2013;110(10):4009-4014.
141. Turashvili G, Brogi E. Tumor heterogeneity in breast cancer. Front Med. 2017;4:227.
142. Delgado-Goñi T, Julià-Sapé M, Candiota AP, Pumarola M, Arús C. Molecular imaging coupled to pattern recognition distinguishes response to temo- zolomide in preclinical glioblastoma. NMR Biomed. 2014;11:1333-1345.
143. Ciezka M, Acosta M, Herranz Sotoca C, et al. Development of a transplantable tumour model from a spontaneously grown glial mass in a genetically engineered mouse and its characterisation by MRI/MRS/MRSI. J Neuro-Oncol. 2016;129(1):67-76.
144. Ferrer-Font L, Arias-Ramos N, Lope-Piedrafita S, et al. Metronomic treatment in immunocompetent preclinical GL261 glioblastoma: effects of cyclophosphamide and temozolomide. NMR Biomed. 2017;30(9). https://doi.org/10.1002/nbm.3748
145. Ferrer-Font L, Villamanan L, Arias-Ramos N, et al. Targeting protein kinase CK2: evaluating CX-4945 potential for GL261 glioblastoma therapy in immunocompetent mice. Pharmaceuticals. 2017;10(1):pii E24.
146. Karman J, Ling C, Sandor M, Fabry Z. Initiation of immune responses in brain is promoted by local dendritic cells. J Immunol. 2004;173(4):2353-2361.
147. Zhu H, Barker PB. MR spectroscopy and spectroscopic imaging of the brain. Methods Mol Biol. 2011;711:203-226.
148. Garcia-Figueiras R, Baleato-Gonzalez S, Padhani AR, et al. Proton magnetic resonance spectroscopy in oncology: the fingerprints of cancer? Diagn Intervent Radiol. 2016;22(1):75-89.
149. Gillies RJ, Morse DL. In vivo magnetic resonance spectroscopy in cancer. Ann Rev Biomed Eng. 2005;7:287-326.
150. Bogner W, Hangel G, Esmaeili M, Andronesi OC. 1D-spectral editing and 2D multispectral in vivo 1H-MRS and 1H-MRSI—methods and applications. Anal Biochem. 2017;529:48-64.
151. Posse S, Otazo R, Dager SR, Alger J. MR spectroscopic imaging: principles and recent advances. J Magn Reson Imaging. 2013;37(6):1301-1325.

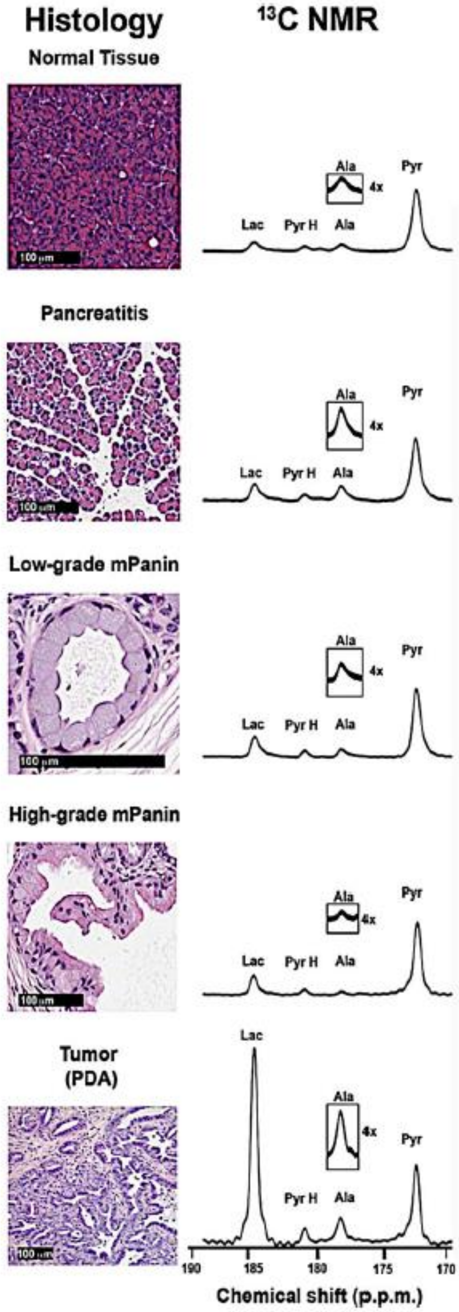

FIGURE 1. Hyperpolarized 13C MRSI spectra acquired at different stages of progression in GEMs prone to develop pancreatic cancer. The predominant lesion histology pattern is shown on the left. The 13C hyperpolarized spectra on the right were selected from an MRSI grid following the injection of hyperpolarized [1-13C] Pyr. Both lac/Pyr and lac/alanine ratios increase with progression. PDA, pancreatic ductal adenocarcinoma; mPanin, murine pancreatic intraepithelial neoplasia. Modified from reference 23 (https://creativecommons.org/licenses/by/4.0/)

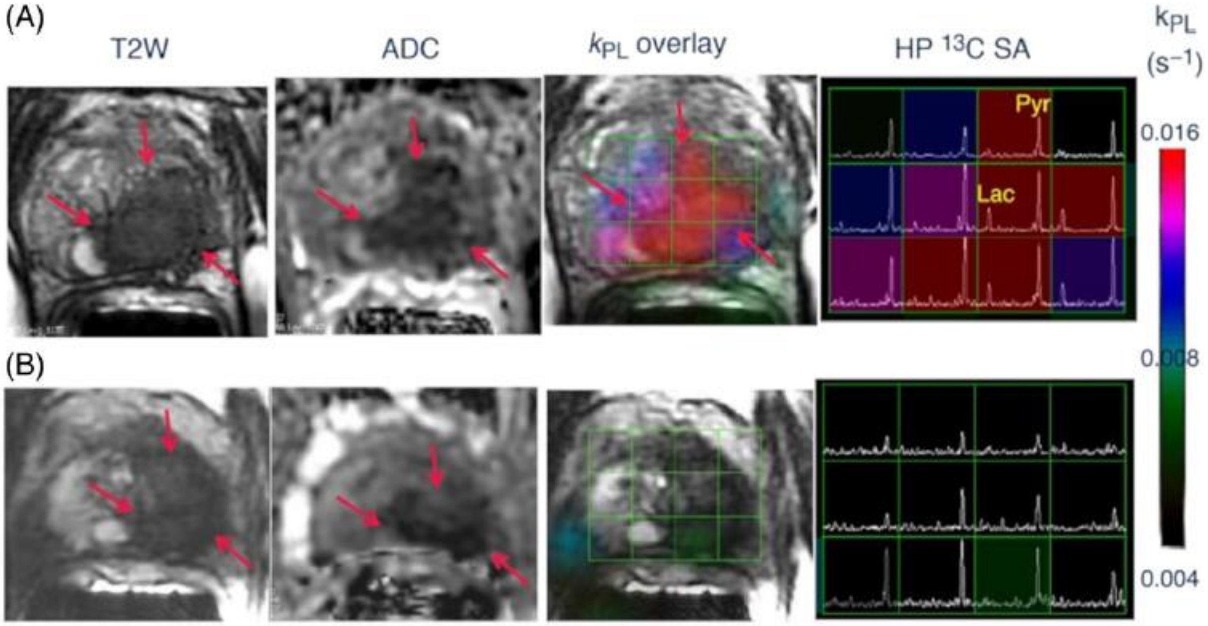

FIGURE 2. Representative axial T2W anatomic image, corresponding water ADC image and T2W image with an overlaid Pyr-to-lac metabolic flux (kPL) image and corresponding hyperpolarized 13C MRSI spectral array (SA) for a 52-year-old prostate cancer patient with extensive high- grade prostate cancer before therapy A, and 6 weeks after initiation of androgen ablation and chemotherapy B, before treatment, the region of prostate cancer can be clearly seen (red arrows) as a reduction in signal on the T2W and ADC images, and increased hyperpolarized lac and associated kPL flux on hyperpolarized 13C MRSI. After initiation of androgen deprivation therapy there was a significant reduction in hyperpolarized lac and kPL fell to normal levels, with only a modest treatment effect on prostate volume and ADC. Taken from reference 27

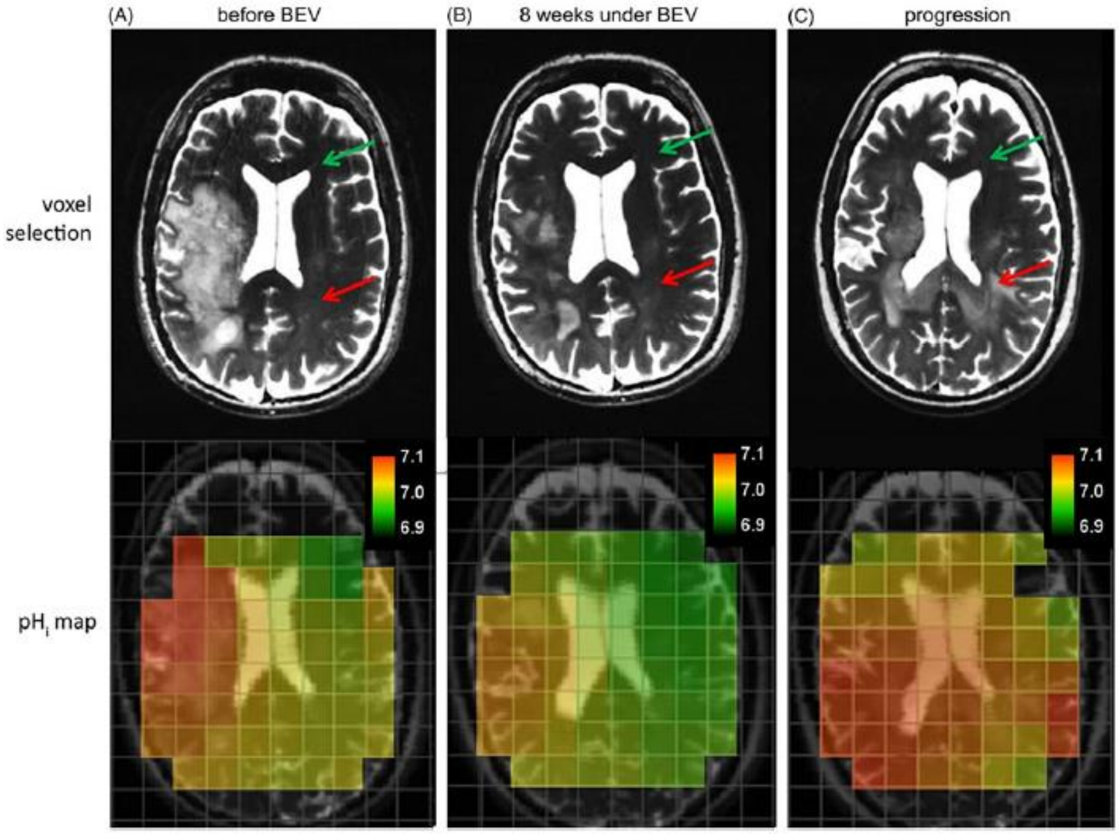

FIGURE 3. Brain and tumour pHi maps were calculated using the inorganic phosphate signal chemical shift of multivoxel 31P MRS data and were colour coded (bottom row). The area of interest for voxel selection defined on standard MRI sequences is demonstrated with arrows (parieto-occipital selection, red, marks subsequent tumour position; frontal selection, green, marks control). A small number of spectra outside the ROI, close to the skull/brain interface, suffered from artefacts and were removed. Taken from reference 39

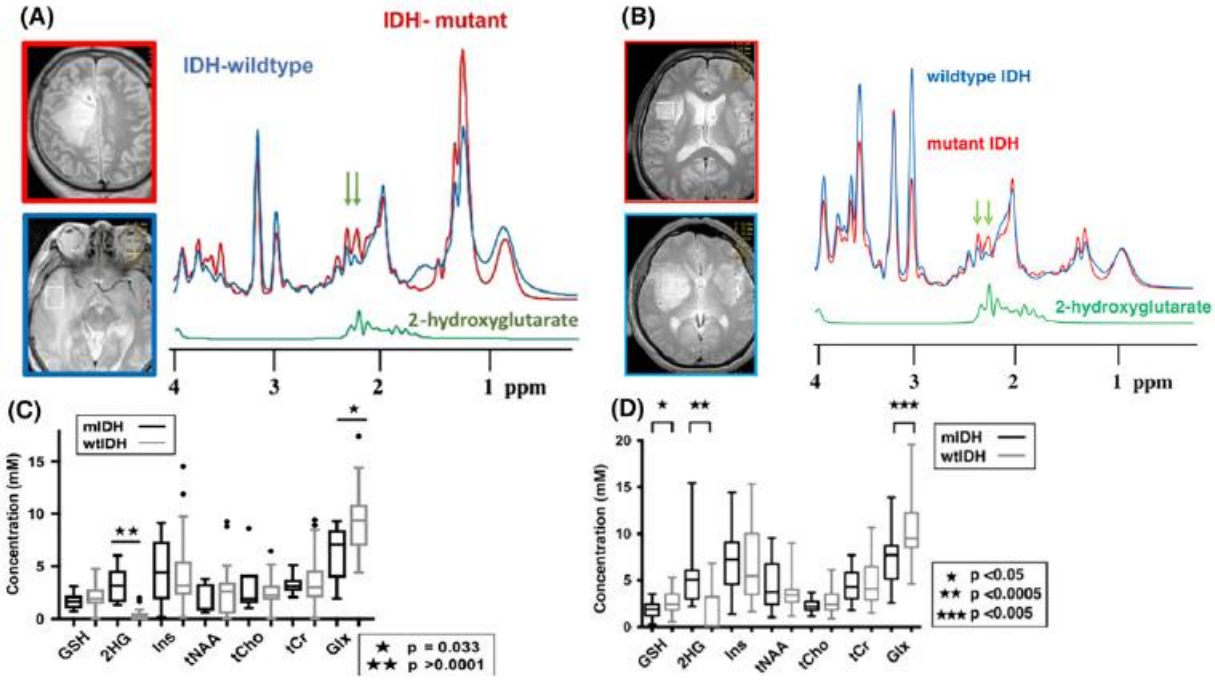

FIGURE 4. Pattern variations in gliomas (A, C, GB; B, D, grade II-III glioma). A, B, representative SV 1H-MRS of mutant and wt. C, quantified metabolites in wt and mutant IDH GB. D, quantified metabolites in wt and mutant IDH grade II-III gliomas. Figure adapted from references 63 (https://creativecommons.org/licenses/by/4.0/) and 64

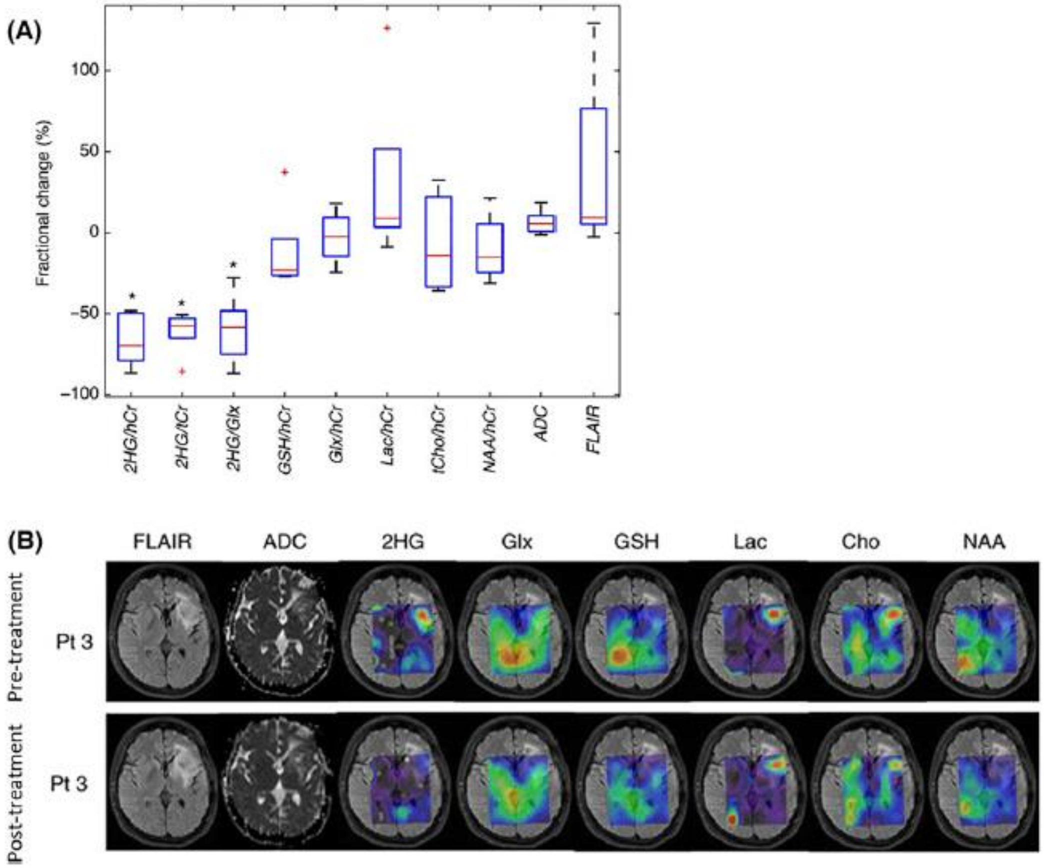

FIGURE 5. A, treatment-induced changes in mutant IDH patients. Boxplot of the fractional changes for the mean values averaged over the tumour ROI. The box size represents the first and third quartiles, and the horizontal red line indicates the median. Statistically significant changes are indicated by asterisks ($P < 0.05$). B, regional metabolic changes induced by treatment in a responding patient with the IDH mutation (patient 3, Pt 3). Adapted from reference 65 (https://creativecommons.org/licenses/by/4.0/)

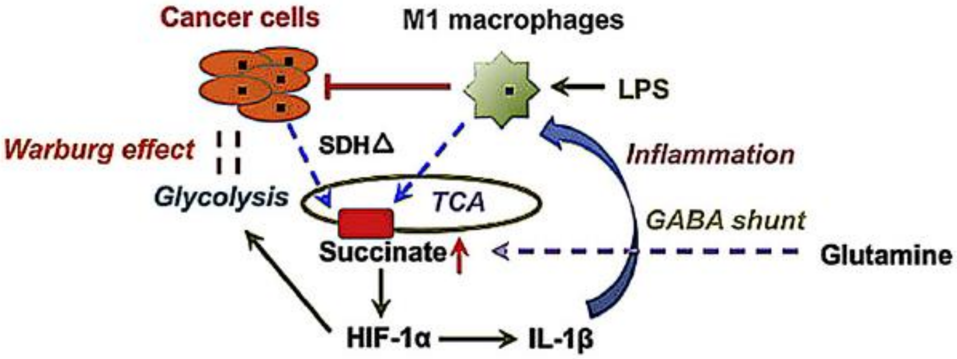

FIGURE 6. Succinate homeostasis is controlled by multiple factors in the cancer- immunity cycle cross-talk. Succinate elevations through upstream SDH mutations in cancer cells can promote downstream HIF- 1α stabilization, which induces the key pro- inflammatory cytokine, IL-1β. IL-1β can polarize macrophages to the M1 sub-type, which gives them the capacity to damage tumour cells. HIF-1α driven by elevated succinate can promote glycolysis in cancer cells. Also, glutamine contributes to succinate levels through the GABA (gamma aminobutyric acid) shunt pathway, although glutamine has opposite roles in cancer cells and macrophages. Taken from reference 70.

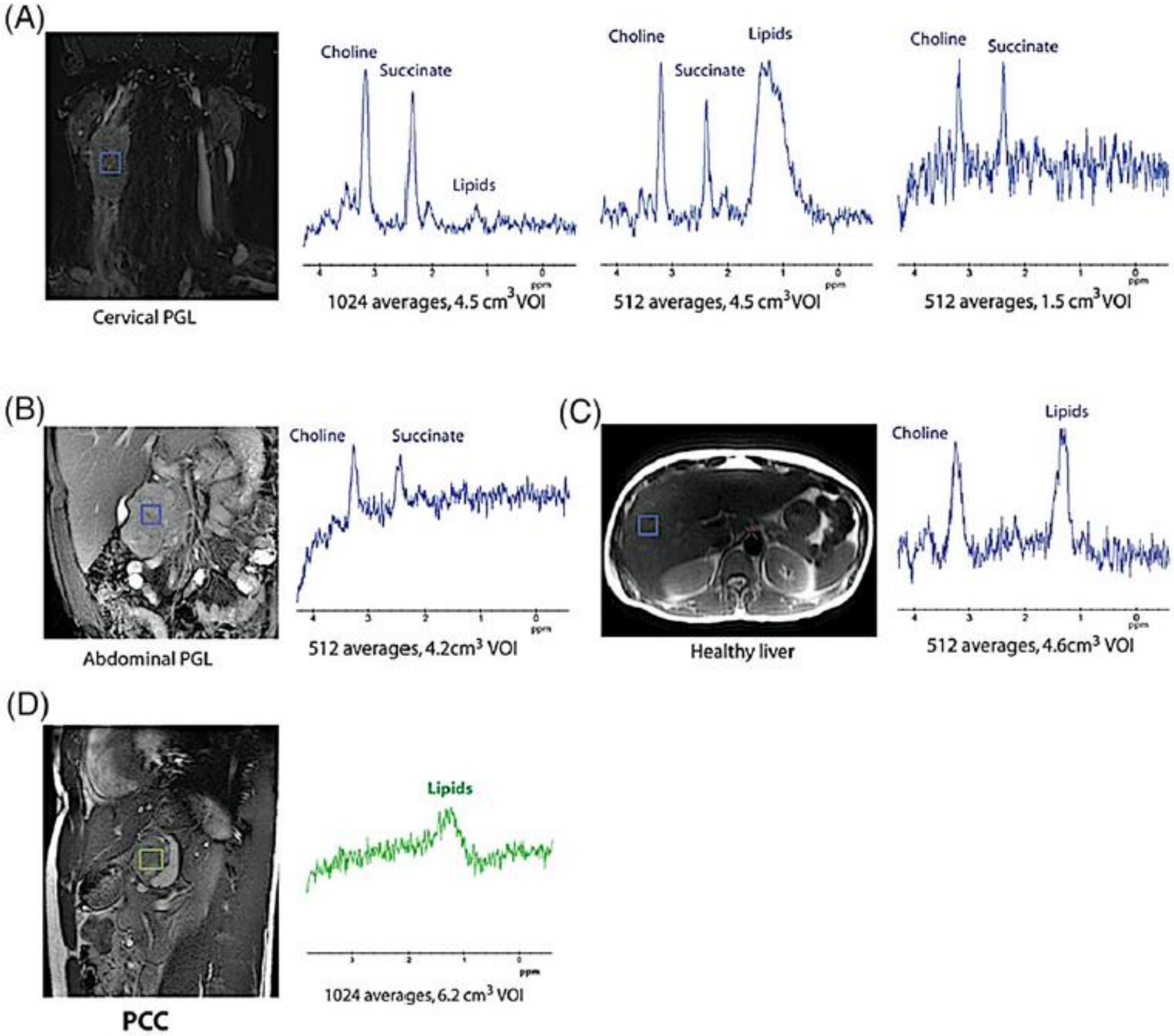

FIGURE 7. SUCCES in a patient with an SDHB gene mutation. A, 1H-MRS spectra of the right cervical paraganglioma (PGL) of patient 1. A succinate peak was detected in the cervical PGL with two different averages (1024 and 512) and two different VOI sizes (4.5 and 1.5 cm3). B, applying the PRESS sequence to the abdominal tumour mass of the same patient permits detection of a succinate peak. C, in the healthy liver, the absence of a succinate peak demonstrates the specificity of the method. D, patient with a pheochromocytoma (PCC) without the SDHx mutation. Adapted from reference 71.

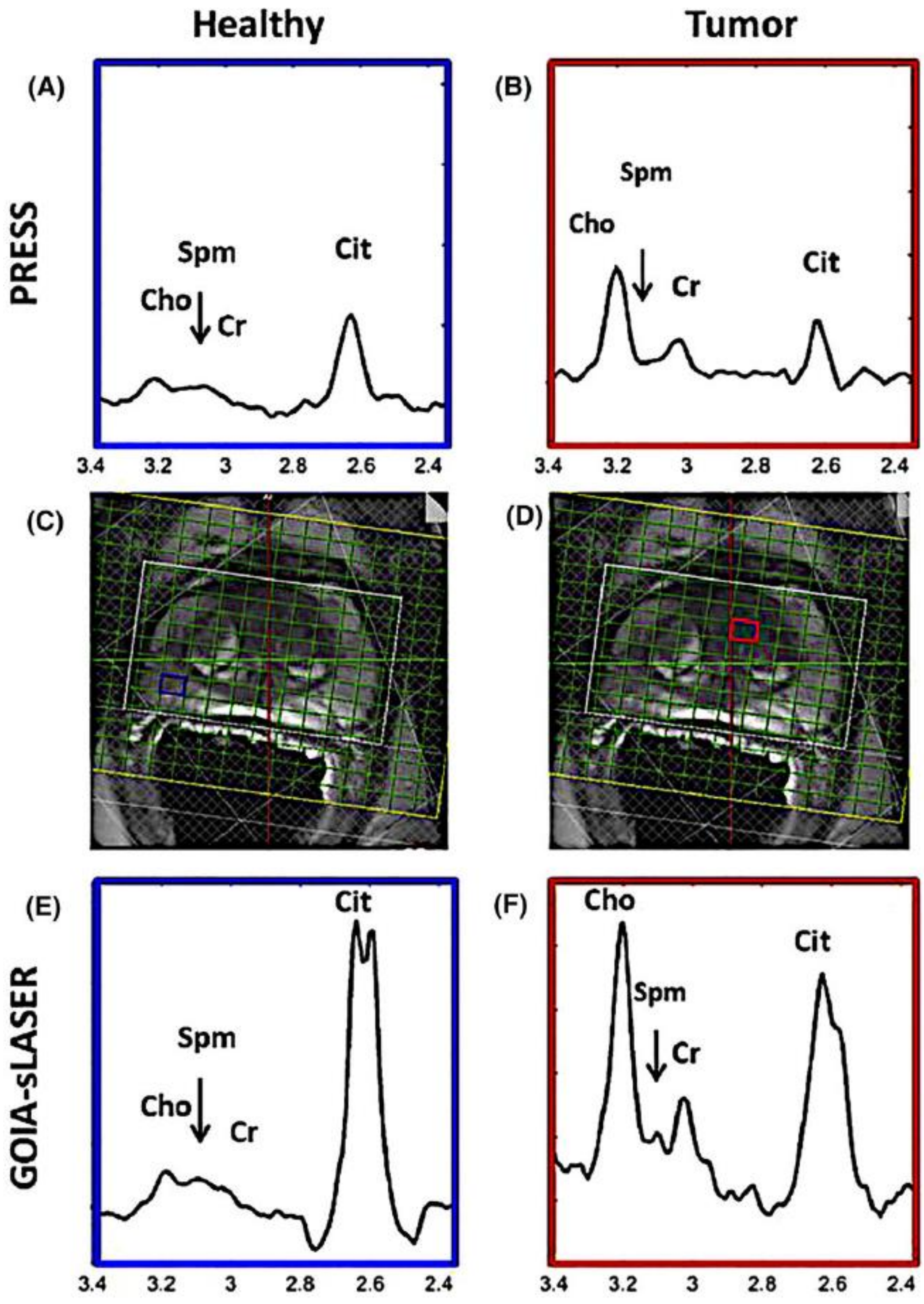

FIGURE 8. MRSI data of a patient with a Gleason score 3 + 4 prostate cancer in the left transition zone. The patient was measured with both the PRESS and GOIA-sLASER sequences at 3 T. on the T2W images with the spectroscopy grid (C, D), the locations of the normal voxel and tumour voxel are indicated. Representative spectra from normal appearing tissue acquired with PRESS A, and GOIA-sLaser E, and tumour tissue acquired with PRESS B, and GOIA-sLaser F, illustrate the differences in metabolite signal intensities between healthy and tumour tissue. The PRESS data

were measured at TR/TE = 1020/145 ms and the GOIA-sLASER data was measured at TR/TE = 1020/88 ms. indicated are the main prostate metabolites: Cit, Cho, Spm and Cr. Healthy spectra A and E have the same scaling, and tumour spectra B and F have the same scaling, showing the increase in SNR of the GOIA-sLASER sequence compared with PRESS. Note that, because of their different distances from the endorectal coil used, scalings between tumour and healthy voxel were different. Taken from reference 81 (https://creativecommons.org/licenses/by-nc-nd/4.0/)

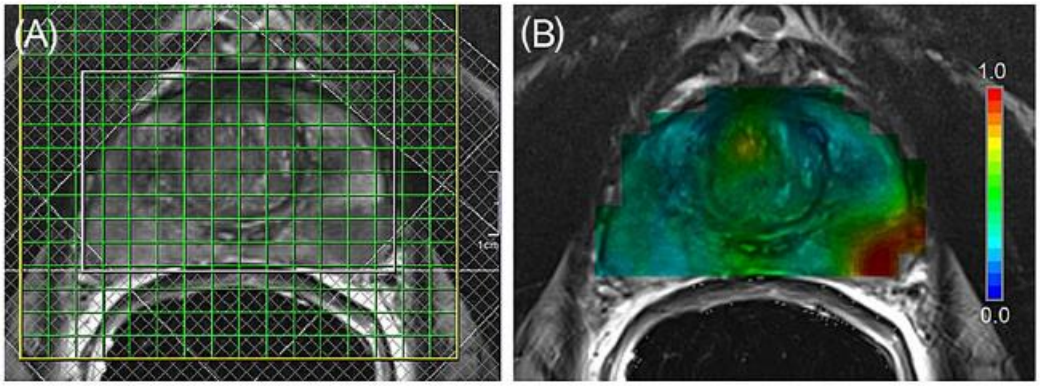

FIGURE 9. A, T2W image of the prostate of a 57-year-old man with biopsy-proven prostate cancer in the left peripheral zone. The MRSI grid is plotted over the prostate, as are the outer volume saturation slabs. B, an example of a tumour probability map based on MRSI data that could be presented to a clinician. In this case, the probability map is based on the Cho + Cr to Cit ratio (colour coded bar on right). Taken from reference 90

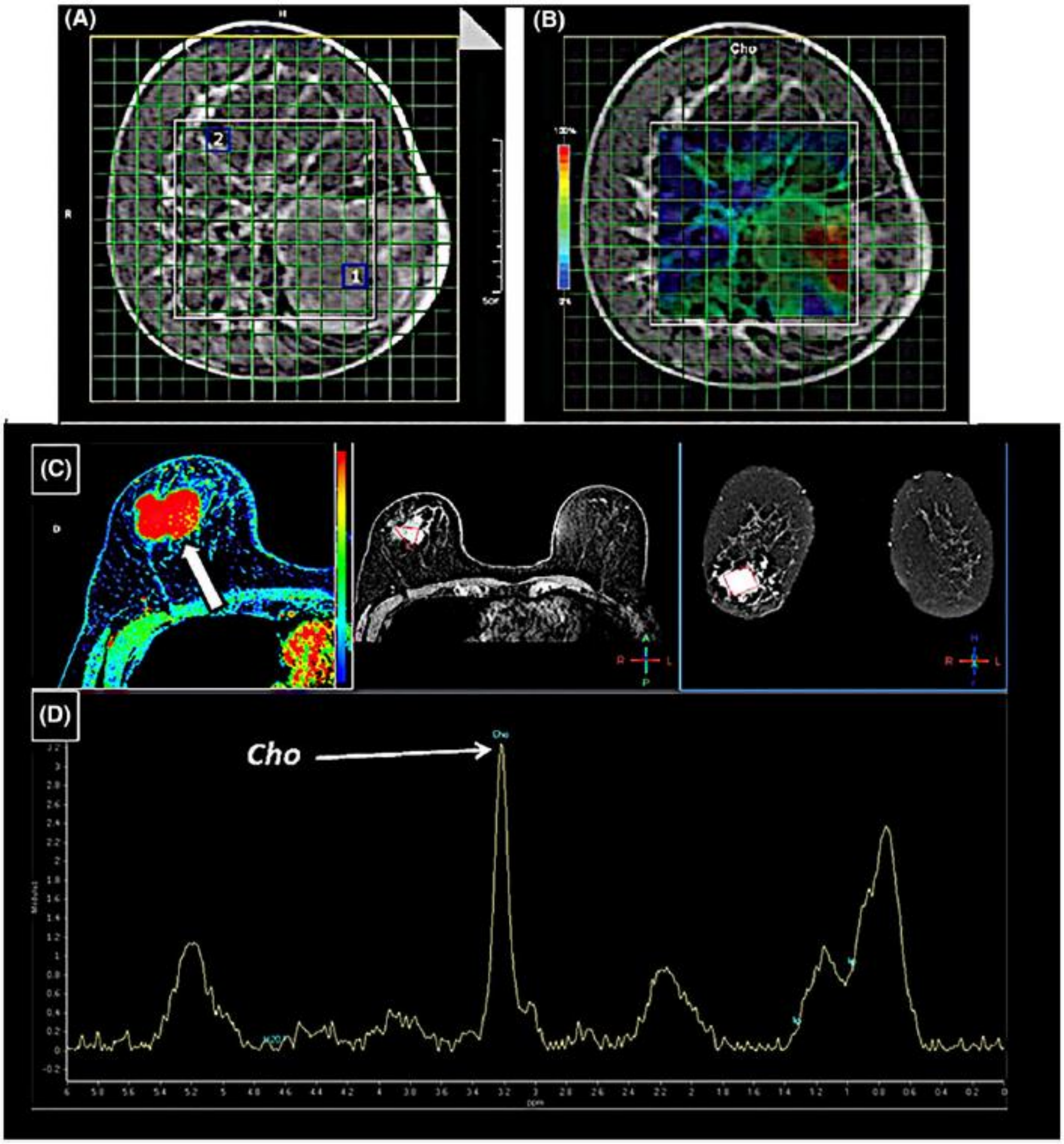

FIGURE 10. A, MRSI grid for a breast evaluation. B, overlay of MRSI tCho map superimposed on an MRI image of a breast with a large tumour. Adapted and modified from reference 93. Voxel 1 inside the tumour presented a high Cho level, while voxel 2 (outside the tumour) had no Cho signal detectable. C, D, breast MRS from a 67-year-old woman with a suspicious right breast lesion (solid arrow in C) that shows high vascularization in maximum relative enhancement parametric map and maximum intensity projection images derived from DCE-MR imaging (C) and a marked Cho peak in SV MRS (D), both findings consistent with malignant origin. Notice the positioning of the VOI in C (middle and right images). Papillary breast carcinoma was confirmed on core biopsy. Taken from reference 94.

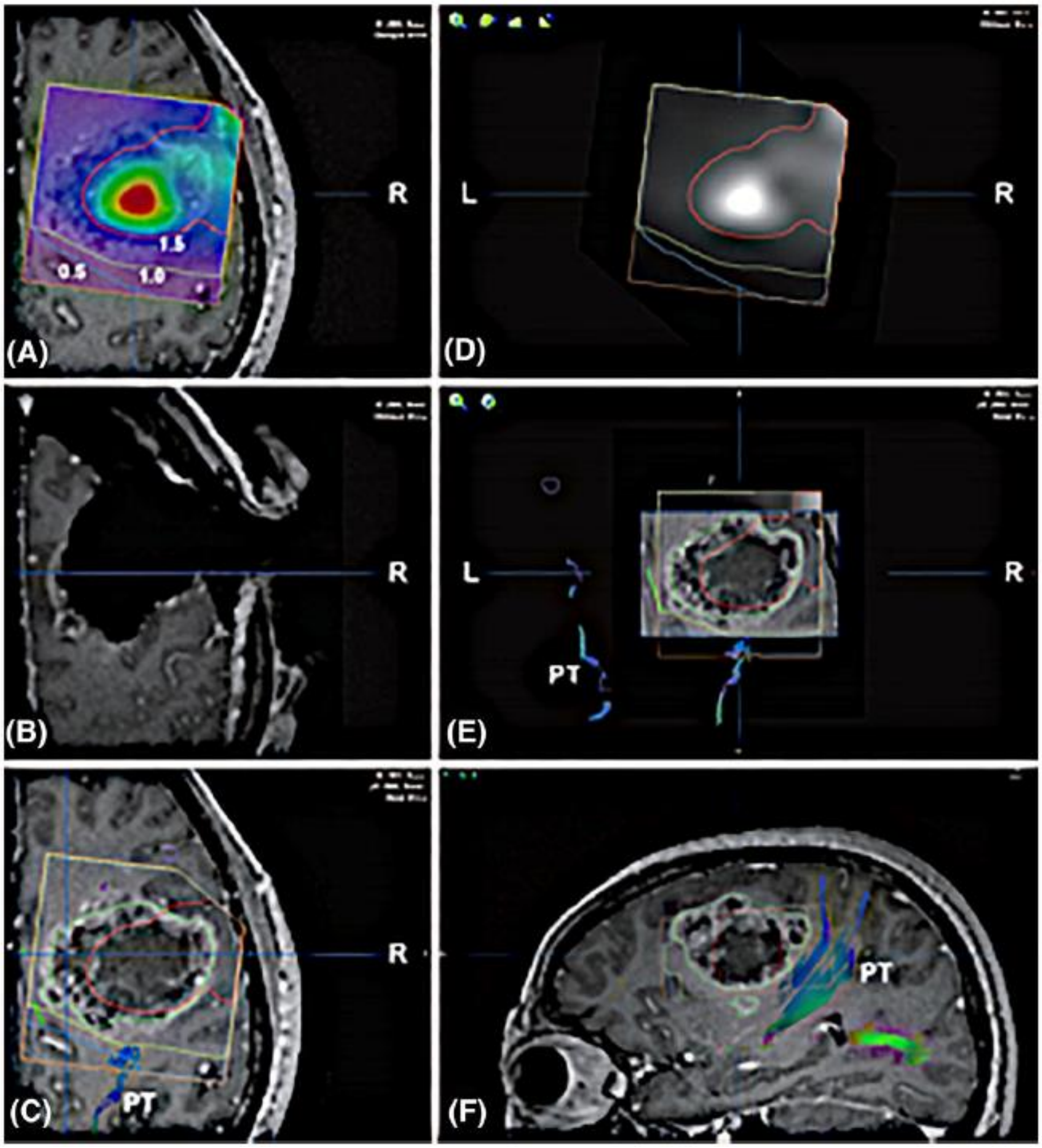

FIGURE 11. Case of a GB patient investigated at 3 T for maximizing resection of the metabolically abnormal region. The process of converting and merging 3D 1H-MRS images (TE = 135 ms) with structural images is summarized. A, 3D 1H-MRS revealed different metabolic margins generated for CNIs (defined as total tCho/NAA area ratios as in reference 97) of 0.5, 1.0 and 1.5, which were transferred into iPlan 3.0 cranial. The pseudocolour maps were then generated. B, postoperative MR image. C, functional MRI and diffusion tensor imaging located the hand motor areas and pyramidal tracts (PTs). D, E, the contour line for a CNI of 1.0 was adjacent to the PTs. red, 1.5; yellow, 1.0; blue, 0.5. To achieve a maximal safe resection, the extent of resection was carried as close as possible to the metabolic margin generated for a CNI of 1.0. F, sagittal view revealing the relationship of the PTs and metabolic margins. A safe margin of 0.8 mm was set to avoid further neurological deficits, even though this margin was near the PTs. a subtotal resection was achieved in this patient. Taken from reference 98

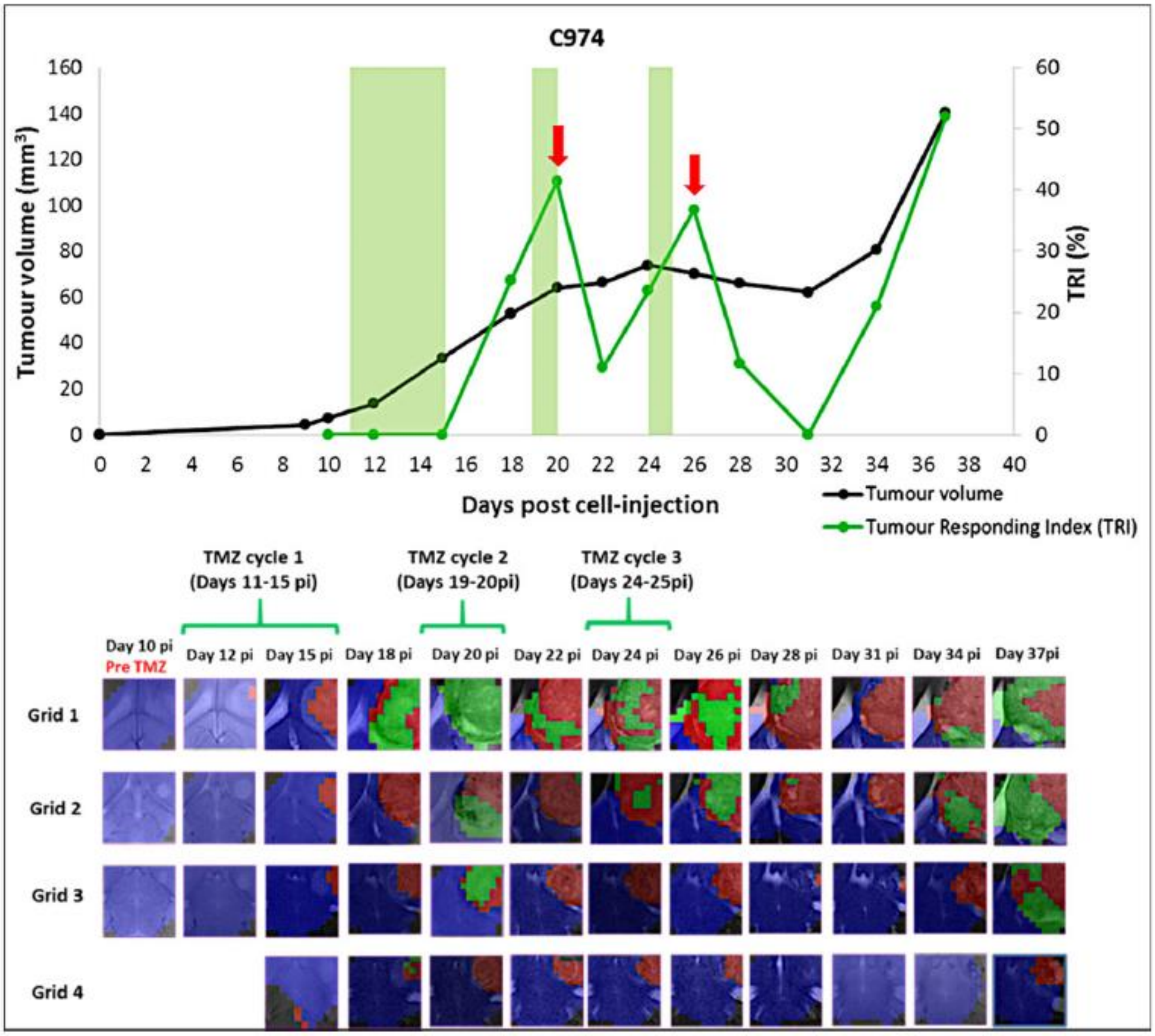

FIGURE 12. Graphical representation of the tumour volume evolution and the percentage of responding 'green' pixels obtained after source analysis of MRSI data acquired in the multislice set for case C974 (intermediate response case). The green shaded columns indicate TMZ administration periods. For chosen time points, the evolution of the nosological images obtained with the semi-supervised source extraction system is shown in four rows of colour coded grids, superimposed on the T2W MRI for each slice. Green brackets indicate TMZ administration periods. A cyclical pattern of response was observed, marked by the red arrows in the graphical representation. Taken from reference 133 (https:// creativecommons.org/licenses/by/4.0/)